HHS Public Access

Author manuscript

Cell Rep. Author manuscript; available in PMC 2020 April 20.

Published in final edited form as:

Cell Rep. 2020 March 10; 30(10): 3448–3465.e8. doi:10.1016/j.celrep.2020.02.054.

Neurokinin-1 Receptor Signaling Is Required for Efficient Ca^{2+} Flux in T-Cell-Receptor-Activated T Cells

Adrian E. Morelli[1,2,3,13], **Tina L. Sumpter**[3,4,13], **Darling M. Rojas-Canales**[5], **Mohna Bandyopadhyay**[4], **Zhizhao Chen**[6], **Olga Tkacheva**[4], **William J. Shufesky**[1,2], **Callen T. Wallace**[7,8], **Simon C. Watkins**[3,7,8], **Alexandra Berger**[9], **Christopher J. Paige**[9], **Louis D. Falo Jr.**[4,8,10,11,12,14], **Adriana T. Larregina**[3,4,8,14,15,*]

[1]Thomas E. Starzl Transplantation Institute, University of Pittsburgh, School of Medicine, Pittsburgh, PA, USA

[2]Department of Surgery, University of Pittsburgh, School of Medicine, Pittsburgh, PA, USA

[3]Department of Immunology, University of Pittsburgh, School of Medicine Pittsburgh, PA, USA

[4]Department of Dermatology, University of Pittsburgh, School of Medicine, Pittsburgh, PA, USA

[5]Flinders University, College of Medicine and Public Health, Adelaide, SA, Australia

[6]Hubei Key Laboratory of Medical Technology on Transplantation, Transplant Center, Institute of Hepatobiliary Diseases, Zhongnan Hospital, Wuhan University, Wuhan, Hubei, China

[7]Department of Cell Biology and Center for Biological Imaging, University of Pittsburgh, School of Medicine, Pittsburgh, PA, USA

[8]The McGowan Center for Regenerative Medicine, Pittsburgh, PA, USA

[9]Ontario Cancer Institute, Princess Margaret Hospital, Toronto, ON, Canada

[10]Department of Bioengineering, University of Pittsburgh Swanson School of Engineering, Pittsburgh, PA, USA

[11]The University of Pittsburgh Clinical and Translational Science Institute, Pittsburgh, PA, USA

[12]The UPMC Hillman Cancer Center, Pittsburgh, PA, USA

[13]These authors contributed equally

[*]Correspondence: adrianal@pitt.edu.

AUTHOR CONTRIBUTIONS

A.E.M. conducted *in vitro* experiments of T cell biasing, FACS and ImageStream analysis, generated the BM chimeras, analyzed data, and contributed to the manuscript writing. T.L.S. and M.B. conducted experiments and data analysis on Ca^{2+} flux and T cell signaling. D.M.R.-C. performed experiments of Ca^{2+} signaling and qRT-PCR. Z.C., O.T., and W.J.S. performed FACS, western blots and ImageStream analysis, and histological analysis on tissue sections. A.B. and C.J.P. generated the B6 $NK1R^{KO}$ and *Tac1/4*$^{Double\ KO}$ mice and provided intellectual input. C.T.W. and S.C.W. assessed Ca^{2+} flux in T cells by live-cell microscopy. L.D.F. collaborated with the experimental planning and provided intellectual input in data interpretation. A.T.L. planned and supervised the experiments, conducted FACS analysis and *in vivo* studies with BM chimeras, analyzed data, and supervised the writing of the manuscript.

SUPPLEMENTAL INFORMATION

Supplemental Information can be found online at https://doi.org/10.1016/j.celrep.2020.02.054.

DECLARATION OF INTERESTS

The authors declare no competing interests.

[14]Senior author

[15]Lead Contact

SUMMARY

Efficient Ca^{2+} flux induced during cognate T cell activation requires signaling the T cell receptor (TCR) and unidentified G-protein-coupled receptors (GPCRs). T cells express the neurokinin-1 receptor (NK1R), a GPCR that mediates Ca^{2+} flux in excitable and non-excitable cells. However, the role of the NK1R in TCR signaling remains unknown. We show that the NK1R and its agonists, the neuropeptides substance P and hemokinin-1, co-localize within the immune synapse during cognate activation of T cells. Simultaneous TCR and NK1R stimulation is necessary for efficient Ca^{2+} flux and Ca^{2+}-dependent signaling that sustains the survival of activated T cells and helper 1 (Th1) and Th17 bias. In a model of contact dermatitis, mice with T cells deficient in NK1R or its agonists exhibit impaired cellular immunity, due to high mortality of activated T cells. We demonstrate an effect of the NK1R in T cells that is relevant for immunotherapies based on pro-inflammatory neuropeptides and its receptors.

Graphical Abstract

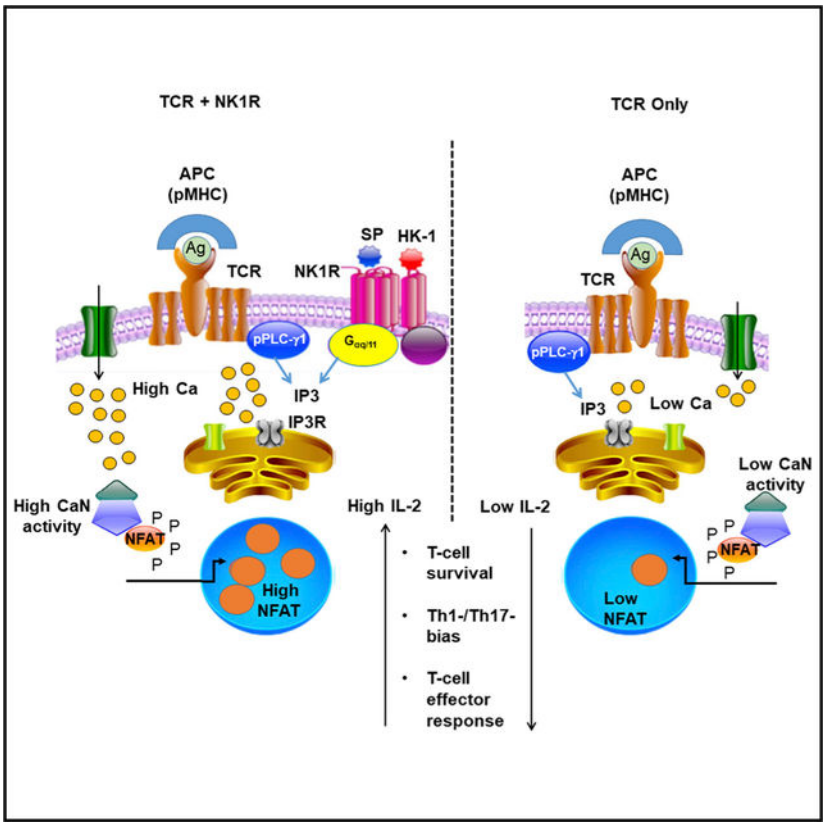

In Brief

The neurokinin 1 receptor (NK1R) induces Ca^{2+} flux in excitable cells. Here, Morelli et al. show that NK1R signaling in T cells promotes optimal Ca^{2+} flux triggered by TCR stimulation, which is

necessary to sustain T cell survival and the efficient Th1- and Th17-based immunity that is relevant for immunotherapies based on pro-inflammatory neuropeptides.

INTRODUCTION

Cellular adaptive immunity relies on cognate activation of T cells by APC within the immune synapse (Benvenuti, 2016; Grakoui et al., 1999). Following cognate signaling, the T cell receptor (TCR) triggers a rapid increase in the concentration of cytosolic Ca^{2+} (Feske, 2007; Fracchia et al., 2013). This surge of cytosolic Ca^{2+} promotes the enzymatic activity of calcineurin, which dephosphorylates Ca^{2+}-dependent NFAT1, NFAT2, and NF-kB (Ishihara and Schwartz, 2011). These factors are key for the synthesis of IL-2, a cytokine that sustains proliferation, maturation, and survival of T cells (Gwack et al., 2007; Hogan et al., 2003; Ishihara and Schwartz, 2011).

The rapid increase in cytosolic Ca^{2+} depends on its release from the pool of Ca^{2+} stored in the ER. Depletion of Ca^{2+} from the ER activates the “store-operated Ca^{2+} entry” (SOCE) mainly through the “Ca^{2+} release-activated Ca^{2+}” (CRAC) channels that provide sustained entry of extracellular Ca^{2+} (Feske, 2007; Fracchia et al., 2013; Gwack et al., 2007; Hogan et al., 2003).

Release of intracellular Ca^{2+} depends on the activation of the phospholipase C (PLC) subunits γ1 and β1 (Kawakami and Xiao, 2013). In T cells, PLC-γ1 activation is triggered by TCR stimulation, and PLC-β1 activation requires signaling via a G-protein-coupled receptor (GPCR) that recruits $G_{\alpha q/11}$ proteins (Bueno et al., 2006; Sánchez-Fernández et al., 2014; Stanners et al., 1995; Zhang and Shi, 2016). To our knowledge, the GPCRs that cooperates with the TCR to promote Ca^{2+} flux in activated T cells remains to be identified.

The neurokinin-1 receptor (NK1R) belongs to the family of GPCRs that signal via $G_{\alpha q/11}$ subunits to promote Ca^{2+} flux in excitable and non-excitable cells (Boyd et al., 1991; Ge et al., 2019; Kwatra et al., 1993; Miyano et al., 2010). Substance P (SP) and hemokinin-1 (HK-1) are pro-inflammatory neuropeptides of the tachykinin family that bind with high affinity to the NK1R and provide adjuvant effect to innate and adaptive immune responses (Bozic et al., 1996; Janelsins et al., 2009, 2013; Mathers et al., 2007; Steinhoff et al., 2014; Taracanova et al., 2017).

In the central nervous system, SP is secreted by neurons and microglial cells (Endo et al., 2016; Zhang et al., 2007). In peripheral tissues, SP is released by sensory nerve endings and to a lesser extent by resident cells and migratory leukocytes including T cells, whereas HK-1 is preferentially synthesized by immune cells (Janelsins et al., 2013; Steinhoff et al., 2014; Sumpter et al., 2015; Zhang et al., 2000). SP is a mediator of neuroinflammation, whereas HK-1 promotes immune responses and is necessary for survival of B- and T cell precursors (Steinhoff et al., 2014; Zhang et al., 2000; Zhang and Paige, 2003). SP and HK-1 stimulate T cell immunity via agonistic binding of the NK1R (Berger and Paige, 2005; Bozic et al., 1996; Weinstock, 2004). In this regard, we have described that signaling via the NK1R *in vivo* enhances the survival and the APC function of dendritic cells (DCs) and promotes T

helper 1 (Th1)- and T cytotoxic (Tc) 1-biased immunity (Janelsins et al., 2009, 2013; Mathers et al., 2007).

Here, we demonstrate that NK1R-signaling plays a previously unknown relevant role during cognate activation of T cells. We confirm that T cells express the full-length NK1R (f-NK1R), synthesize SP and HK-1, and the NK1R and its agonists co-localize within or in proximity to the immune synapse between T cells and Ag-loaded APC. NK1R-signaling, per se, triggers Ca^{2+} flux in T cells. During TCR-mediated activation, expression of the NK1R is necessary for optimal Ca^{2+} flux and the subsequent signaling of the intracellular pathways that lead to IL-2 secretion and T cell survival. These effects are absent or substantially reduced in T cells deficient in the NK1R, its ligands SP or HK-1, or following pharmacological inhibition of the NK1R. In addition, NK1R-signaling supports Th1 cell-survival and Th17 bias. Consequently, mice with T cells lacking the NK1R or its natural agonists exhibited deficient T cell immunity in a model of skin contact dermatitis, and this effect was associated with high mortality of T cells during priming in skin-draining lymph nodes and effector T cells homed in the skin.

RESULTS

T Cells Express Full-Length NK1R that Colocalizes with Its Agonists in the Immune Synapse

The rapid mobilization of intracellular Ca^{2+} triggered by cognate activation of T cells requires signaling through the TCR and a GPCR associated to $G_{\alpha q/11}$ subunits (Stanners et al., 1995). However, to our knowledge, the GPCR that promotes Ca^{2+} flux in activated T cells remains to be identified. The NK1R, a GPCR that recruits $G_{\alpha q/11}$ proteins, induces Ca^{2+} flux in excitable and non-excitable cells (Ge et al., 2019; Miyano et al., 2010; Zhang et al., 2007). Although the NK1R is expressed by mouse and human T cells, its role in Ca^{2+} flux during TCR stimulation of T cells has not been explored (Lai et al., 1998; Reinke et al., 2006; Siebenhaar et al., 2007; Steinhoff et al., 2014; Vilisaar et al., 2015; Weinstock, 2015). Fluorescence-activated cell sorting (FACS) analysis of splenic T cells from wild-type (WT) and $NK1R^{KO}$ mice confirmed that CD4 and CD8 T cells express surface NK1R (Figure 1A). The NK1R Ab used was specific against the extracellular domain of the NK1R, and its labeling on $NK1R^{KO}$ T cells included as controls was similar to that of irrelevant IgG (Figure 1A).

Two isoforms of the NK1R have been described, the f-NK1R and the C-terminus-truncated (t-NK1R) variants (Lai et al., 2006). Whereas f-NK1R-signaling promotes binding of the f-NK1R to $G_{\alpha q/11}$ subunits and causes increase in cytosolic Ca^{2+}, agonistic binding to the t-NK1R does not (Spitsin et al., 2018; Tuluc et al., 2009). Although the NK1R is expressed in T cells, it is unknown if both isoforms are present in T cells and how their level of expression changes during TCR-activation. Thus, we assessed the two NK1R isoforms in mouse T cells, left untreated or after 24 h stimulation with CD3 and CD28 agonistic Ab. We demonstrated by FACS (intracellularly) and western blot analysis that naive and TCR-activated CD4 and CD8 T cells express similar amounts of the f-NK1R (Figures 1B and 1C), the latter detected with an Ab directed to the C terminus domain only present in the f-NK1R variant. The t-NK1R isoform was assessed with an Ab against the extracellular N-terminus

motif of the NK1R that is present in both variants of the receptor, which differ in their molecular weights. In this case, the NK1R was detected on T cells by western blot as a single band of ~75 kDa that corresponds to the glycosylated form of the f-NK1R. Bands of lower molecular weight, indicative of the t-NK1R isoform, were not detected (Figure 1C). Thus, naive CD4 and CD8 T cells express the f-NK1R, which is the functional variant of the receptor, and its expression does not change upon T cell activation by TCR signaling.

Both T cells and DC express NK1R protein or transcripts for SP and HK-1 (Janelsins et al., 2009; Lambrecht et al., 1999; Mathers et al., 2007). Therefore, we tested if the NK1R and its agonists participate in cognate activation of T cells. We investigated by ImageStream analysis the spatial relationship between the NK1R and its agonists during cognate activation of naive T cells by professional APC loaded with Ag. DC generated from WT or $NK1R^{KO}$ C57BL/6 (B6) bone marrow (BM) progenitors (BMDC) were loaded with ovalbumin $(OVA)_{323–339}$ peptide and then co-cultured with OT-II CD4 T cells, the latter specific for the IA^b-$OVA_{323–339}$ complex and labeled with Cell Tracker Violet. As control, OT-II cells were incubated with B6 BMDC without $OVA_{323–339}$. After 2 h, cells were labeled with CD11c Ab for identification of DC in combination with Abs against NK1R, SP, or HK1. Immune synapses were identified by the rearrangement of filamentous actin (F-actin) detected by intracellular labeling with phalloidin. T cell-DC doublets were selected from the cell clusters gate, previously selected from the cells in the focus gate. For quantification of the relative concentration of NK1R, SP, and HK-1 within the area of the T cell-DC synapse, we generated a tight interface mask at the site of contact between the DC and T cell where the rearrangement of F-actin occurred. Within that area, we identified the NK1R, SP, and HK-1 within 8 pixels from the point of cell-to-cell contact (Figures 1D and 1E). The fluorescence intensities of NK1R, SP, and HK-1 labeling at the T cell-DC interphase were significantly higher in the presence of $OVA_{323–339}$ (Figure 1E). Thus, during cognate interaction between T cells and DC, the f-NK1R and its ligands SP and HK-1 concentrate within or next to the immune synapse. Importantly, NK1R expressed by T cells contribute to the fraction of NK1R mobilized to the immune synapse, as segregation of the NK1R inside or near the immune synapse was detected by ImageStream analysis when OT-II T cells were incubated with $NK1R^{KO}$ DCs loaded with $OVA_{323–339}$ (Figure 1F).

NK1R Signaling Triggers Ca^{2+} Flux in T Cells

Next, we tested if agonistic signaling via the NK1R in T cells induces Ca^{2+} flux, an effect mediated through the C terminus of the f-NK1R (Lai et al., 2008). Mouse splenic T cells loaded with the Ca^{2+} flux probes Fluo-4-AM and Fura Red-AM were exposed to increasing concentrations of the synthetic NK1R agonist [$Sar^9Met(O_2)^{11}$]-SP (SarSP) and Ca^{2+} flux was analyzed by a ratiometric assay by FACS. SarSP increased the level of intracellular Ca^{2+} in CD4 and CD8 T cells in a dose-dependent manner (from 10^{-7} to 10^{-8} M), an effect that was less pronounced at a higher concentration (10^{-5} M) (Figure 2A).

In excitable cells, it has been shown that release of Ca^{2+} from intracellular compartments is triggered by NK1R signaling through recruitment of $G_{\alpha q/11}$ proteins (Miyano et al., 2010; Mizuta et al., 2008) whereas influx of extracellular Ca^{2+} occurs by increasing the permeability of voltage-gated channels (Kovac et al., 2006; Rycroft et al., 2007). To confirm

further that NK1R signaling in T cells increases intracellular Ca^{2+} and test if this effect requires recruitment of $G_{\alpha q/11}$ proteins, we used a highly sensitive live-cell imaging approach. CD4 T cells loaded with Fluo-4-AM were incubated with the $G_{\alpha q/11}$ inhibitor YM-254,890 before stimulation with SarSP (10^{-7} M). Our results confirmed that NK1R signaling by SarSP alone triggers Ca^{2+} flux in T cells, and this effect was significantly diminished in T cells treated with YM-254,890 (Figure 2B). Thus, the NK1R on T cells triggers Ca^{2+} flux via $G_{\alpha q/11}$ proteins.

Next, we investigated if NK1R-signaling affects Ca^{2+} flux in T cells following TCR-stimulation triggered by cross-linking of CD3ε Ab bound to the T cells. By ratiometric assays by FACS, we demonstrated that the level of Ca^{2+} flux in TCR-activated wild-type (WT) T cells was significantly higher than that observed in T cells isolated from global $NK1R^{KO}$ mice (Figure 2C) or $NK1R^{KO}$ BM T cell chimeras, the latter a model in which T cells are $NK1R^{KO}$ but the non-T-cell lineages express the NK1R (Figures 2D and S1A–S1C). The reduced Ca^{2+} flux observed in $NK1R^{KO}$ T cells was not due to an intrinsic defect of T cells developed in NK1R-deficient mice, since a similar decrease in Ca^{2+} flux was detected in WT T cells treated with the NK1R antagonists L733,060 or WIN-51,708 before TCR stimulation (Figures 2E and 2F). The experimental conditions used to assess the role of the NK1R in Ca^{2+} flux did not affect T cell viability (Figures S2A and S2B). WT and $NK1R^{KO}$ T cells showed similar Ca^{2+} flux in response to ionomycin, indicating $NK1R^{KO}$ T cells are not intrinsically deficient at increasing cytosolic Ca^{2+} (Figure S2C). Thus, NK1R-signaling promotes optimal Ca^{2+} flux in TCR-activated T cells.

Next, we investigated by ratiometric assays of Ca^{2+} flux by FACS if NK1R signaling affects the release of intracellular Ca^{2+} and the uptake of extracellular Ca^{2+} in TCR-stimulated T cells. To assess the release of intracellular Ca^{2+}, WT and $NK1R^{KO}$ T cells were maintained in Ca^{2+}-free medium and then TCR-stimulated by CD3 Ab cross linking. As expected in such conditions, WT T cells showed a discrete elevation of intracellular Ca^{2+}, an effect that was substantially reduced in $NK1R^{KO}$ T cells (Figure 2G). To investigate if NK1R signaling affects the uptake of extracellular Ca^{2+} regulated by SOCE, T cells maintained in Ca^{2+}-free medium were treated with thapsigargin, a TCR-independent stimulus that induces release of Ca^{2+} from the intracellular compartments that results in activation of SOCE. Thapsigargin caused similar release of intracellular Ca^{2+} in WT and $NK1R^{KO}$ T cells, indicating that $NK1R^{KO}$ T cells are not intrinsically impaired to mobilize Ca^{2+} from the intracellular compartments. Conversely, following addition of Ca^{2+} and CD3 Ab cross linking, $NK1R^{KO}$ T cells displayed lower uptake of extracellular Ca^{2+} than WT T cells (Figure 2H). Thus, in TCR-stimulated T cells the NK1R is relevant for the release of intracellular Ca^{2+} and uptake of extracellular Ca^{2+}, and the latter involves the activation of SOCE.

The previous results pose the question of whether differences in Ca^{2+} flux between WT and $NK1R^{KO}$ T cells are caused directly by NK1R signaling as suggested by the effect of NK1R antagonists on WT T cells (Figures 2E and 2F), or indirectly by reduced expression of TCR, or decrease in TCR downstream signaling that leads to PLC-γ1 phosphorylation in T cells that develop in a NK1R-deficient environment. By FACS analysis, WT and $NK1R^{KO}$ CD4 and CD8 T cells expressed similar amounts of TCRβ, CD3ε and the TCR-accessory molecules CD4 or CD8 (Figure S3A). Likewise, untreated WT and $NK1R^{KO}$ T cells had

similar basal content of ZAP70 and PLC-γ1 by western blot analysis (Figure S3B), and TCR-stimulated WT and $NK1R^{KO}$ T cells showed similar kinetics and levels of phosphorylation of ZAP70 and PLC-γ1 as analyzed by FACS (Figure S3C). Thus, TCR molecules and their downstream signaling are not compromised in mature $NK1R^{KO}$ T cells.

NK1R Signaling Enhances Viability of TCR-ActivatedT Cells

In accord with the reduced Ca^{2+} flux triggered by TCR-signaling in T cells deficient in NK1R, calcineurin activity in $NK1R^{KO}$ T cells stimulated with CD3 Ab was significantly lower than that detected in WT T cells under similar conditions (Figure 3A). As a control, $NK1R^{KO}$ and WT T cells incubated with ionomycin exhibited similar calcineurin activity (Figure 3A), which indicates that $NK1R^{KO}$ T cells are not intrinsically deficient at activating calcineurin. Thus, TCR-mediated activation of T cells requires NK1R-signaling and likely NK1R-agonists released in a autocrine/paracrine fashion for optimal Ca^{2+} flux and calcineurin activation.

Synthesis and secretion of IL-2 and expression of CD25 (IL-2Ra) by TCR-stimulated T cells requires activation and nuclear translocation of Ca^{2+}-dependent NFAT1 and NFAT2, NFκβ-p65, and Ca^{2+}-independent AP-1 (activator protein-1) (cFos/cJun heterodimer) (Ishihara and Schwartz, 2011). The role of the NK1R in the activation of these transcription factors was analyzed in western blots of nuclear and cytoplasmic extracts of WT and $NK1R^{KO}$ T cells following stimulation with CD3 and CD28 Ab. Untreated WT T cells contained relatively low amounts of nuclear NFAT1, NFAT2, and NFκβ-p65, which increased significantly between 30 and 120 min after activation and remained high up to 2–4 h of follow up (Figures 3B and S4A). In contrast, the nuclear content of NFAT1, NFAT2, and NFκβ-p65 remained low in equally treated $NK1R^{KO}$ T cells (Figures 3B and S4B). These findings were not due to lower content of NFAT1, NFAT2, and NFκβ-p65 in $NK1R^{KO}$ T cells, since the cytoplasmic content of these proteins was similar in WT and $NK1R^{KO}$ T cells (Figure S4B). FACS-based analysis of nuclear content of NFAT1 and NFAT2 confirmed that, following stimulation with CD3 and CD28 Ab, $NK1R^{KO}$ T cells translocate into the nuclei substantially less NFAT1 and NFAT2 than WT T cells (Figures S5A–S5C). Under the same conditions, we did not detect, by western blot analysis, differences in the relative amounts of cFos and cJun in nuclear extracts of WT and $NK1R^{KO}$ T cells (Figure 3B). In accordance, $NK1R^{KO}$ T cells secreted significantly less IL-2 than WT T cells after 24-h stimulation with CD3 and CD28 Ab and expressed less CD25 on the surface (Figures 3C and 3D).

Next, we tested if the lower amounts of IL-2 released by TCR-stimulated $NK1R^{KO}$ T cells affect T cell proliferation, activation, and survival. WT T cells and $NK1R^{KO}$ CD4 and CD8 T cells stimulated with CD3 and CD28 Ab for 4 days exhibited similar capacity to proliferate (based on carboxyfluorescein succinimidyl ester [CFSE] dilution) and to become activated (based on $CD44^{hi}$ expression), as assessed by FACS (Figures 3E and 3F). However, $NK1R^{KO}$ T cells were more susceptible to cell death by apoptosis than WT T cells (Figures 3E and S6), which was prevented by addition of IL-2 (Figure 3G). In summary, the NK1R facilitates nuclear translocation of Ca^{2+}-dependent factors required for *il2* transcription, and the subsequent IL-2 secretion and survival of T cells activated by TCR-

signaling. NK1R-deficiency did not cause T cell anergy, since the surviving $NK1R^{KO}$ T cells proliferated as much as WT T cells (Figure 3F).

NK1R Signaling Enhances Th1 Cell Survival and Th17 Bias

Because NK1R-signaling is required for IL-2 secretion and survival of TCR-stimulated T cells, we investigated if NK1R expression also affects polarization of CD4 T cells. For these studies, WT and $NK1R^{KO}$ naive ($CD44^{lo}$ $CD62L^{hi}$) CD4 T cells were stimulated with artificial APC consisting of 4.5-μm iron beads covered with CD3 and CD28 Ab (Dynabeads) under Th1-, Th2-, or Th17-biasing conditions (Sekiya and Yoshimura, 2016). T cell polarization was confirmed by FACS analysis of intracellular cytokines and T cell biasing transcription factors and by quantification by ELISA of cytokine concentrations in culture supernatants. NK1R signaling was required for optimal polarization of CD4 T lymphocytes into Th1 and Th17 cells, whereas lack of the NK1R did not significantly affect Th2 differentiation (Figures 4A–4E). In the absence of the NK1R, proliferating Th1 and Th17 cells produced less IFN-γ and IL-17, respectively (Figures 4A and 4F), and dividing Th1 cells underwent cell death at higher percentages (Figures 4C and 4E).

The physiological relevance of the effects of NK1R-signaling on CD4 T cell-bias was confirmed *in vivo* in a mouse model of 2,4-dinitrochlorobenzene (DNCB)-induced contact dermatitis caused by delayed-type hypersensitivity (DTH), and Th1- and Th17-cell-dependent (Popov et al., 2011). For these studies, $NK1R^{KO}$ and WT mice were sensitized in the skin (abdomen) with DNCB. After 5 days, we compared the amounts of IFN-γ and IL-17 secreted by CD4 T cells isolated from draining (inguinal) lymph nodes. Consistent with the results obtained *in vitro*, T cells from the skin-draining lymph nodes of $NK1R^{KO}$ mice secreted significantly lower amounts of IFN-γ and IL-17 compared to the T cell counterparts isolated from WT mice (Figure 4 G). Together, the *in vitro* and *in vivo* results demonstrate that NK1R-signaling is required for elicitation of optimal Th1 and Th17 responses.

NK1R Agonists Released by T Cells Augment IL-2 Secretion and T Cell Survival

The previous results obtained without natural APC or exogenous NK1R ligands suggest that the NK1R agonists are released by the T cells. Therefore, we tested if T cells synthetize NK1R agonists. We assessed, by real-time quantitative PCR, the content of *Tac1* and *Tac4* transcripts (encoding SP and HK-1, respectively) in mouse T cells stimulated or not with CD3 and CD28 Ab. *Tac1* and *Tac4* mRNA were detected in untreated CD4 and CD8 T cells, increased significantly between 4 and 6 h after stimulation, and returned to basal levels by 24 h (Figure 5A). These findings were confirmed at the protein level by co-culturing Cell Tracker Violet-labeled OT-II T cells with $Tac1/4^{Double\ KO}$ B6 BMDC, unable to produce SP and HK-1, loaded with $OVA_{323–339}$ peptide. After 2-h incubation, ImageStream analysis demonstrated the presence of SP and HK-1 at the site of T cell-DC contact, which indicates that T cells are indeed a source of endogenous SP and HK-1, which concentrate at the T cell-DC synapse (Figure 5B).

We further investigated if SP and HK-1 released by T cells enhance IL-2 secretion in TCR-stimulated T cells. As expected, WT CD4 T cells secreted significantly more IL-2 than WT

CD8 T cells in response to 24-h stimulation with CD3 and CD28 Ab (Figure 5C). IL-2 secretion by WT T cells did not augment by adding physiological concentrations of SP or HK-1 (Figure 5D). By contrast, *Tac1/4*$^{\text{Double}}$ KO or NK1R^{KO} T cells released significantly less IL-2 than WT controls (Figure 5C). In brief, during cognate activation, T cells are a source of SP and HK-1, which in an autocrine fashion promote IL-2 secretion by T cells.

The effects of release of SP and HK-1 by T cells on T cell activation, proliferation, and survival were analyzed by FACS in WT and *Tac1/4*$^{\text{Double KO}}$ T cells after 4 day-stimulation with CD3 and CD28 Ab alone, or plus exogenous SP, HK-1, or both. *Tac1/4*$^{\text{Double KO}}$ T cells proliferated and became activated as much as WT T cells (Figure 6A). However, *Tac1/4*$^{\text{Double KO}}$ T cells exhibited higher percentages of cell death during proliferation (Figures 6B and 6C), an effect that was prevented by addition of HK-1 and to a lesser extent, SP (Figures 6B and 6C). HK-1 and SP exerted an additive effect in preventing T cell death (Figures 6B and 6C). Thus, both HK-1 and SP released by T cells increase survival of T cells activated by TCR-signaling.

The NK1R and Its Agonists SP and HK-1 Support T Cell Survival *In Vivo*

The biological relevance of NK1R expression during T cell priming *in vivo* was analyzed using a mouse model of DNCB-induced contact dermatitis known to be IFN-γ- and IL-17-dependent (Popov et al., 2011). NK1R^{KO} T cells (CD45.2 Thy1.2 congenic) and WT T cells (CD45.2 Thy1.1), both CFSE-labeled, were intravenously (i.v.) injected at 1:1 ratio in CD45.1 B6 mice. 1 and 2 days later, mice were sensitized on the abdominal skin with DNCB or vehicle. Five days after sensitization, cell proliferation, activation, and cell death were FACS-analyzed on the i.v. transferred T cells in the skin-draining lymph nodes (inguinal). Although NK1R^{KO} T cells proliferated and became activated as efficiently as control WT T cells, up to 85% of the dividing T cells deficient in NK1R underwent cell death (Figures 7A and 7B). Thus, NK1R-signaling facilitates T cell survival during T cell priming *in vivo*.

Next, we investigated the fate of NK1R^{KO} effector T cells that survived priming in the lymph nodes and homed in the skin. We used a model of DNCB-induced contact dermatitis in mouse NK1R^{KO} T cell BM chimeras, a system in which T cells are NK1R^{KO} (Figures S1A and S1B). As controls, we used WT T cell BM chimeras where all hematopoietic lineages encode the WT NK1R allele. The percentages of B and total T cells, as well as the CD4, CD8, and CD4 FoxP3 T cell subsets in the spleen were similar in NK1R^{KO} and WT T cell BM chimeras (Figure S1C). Importantly, all T cell BM chimeras were generated in γ-irradiated TCRαβ^{KO} B6 mice to prevent potential contamination with residual WT αβ T cells that survive γ-irradiation in the hosts. Non-irradiated TCRαβ^{KO} B6 mice did not develop cutaneous DTH reactions of contact dermatitis in response to DNCB (Figures S1D and S1E), which rules out the possibility that WT γδ T cells that survive γ-irradiation in the TCRαβ^{KO} hosts may have affected the skin DTH reaction. Following sensitization on the abdominal skin with DNCB or vehicle, and elicitation on the ear skin with DNCB, chimeras with NK1R^{KO} T cells developed a significantly weaker cutaneous DTH reaction than control WT T cell BM chimeras, based on the percentage of ear thickness increase (Figures 7C and 7D). The abrogation of cutaneous DTH reaction in NK1R^{KO} T cell BM chimeras was

sustained up to 96 h following elicitation, which rules out a possibility of a slower kinetics of the DTH reaction (Figure 7D). The lower percentage of ear thickness increase in $NK1R^{KO}$ T cell BM chimeras correlated with a substantial reduction of the leukocyte infiltrate, fewer T cells and more apoptotic T cells at the elicitation site, as compared to control chimeras (Figures 7E–7G).

Finally, to assess to what extent the release of SP and HK-1 by T cells accounts for the contact dermatitis induced, we conducted similar experiments using mouse *Tac1/4*$^{\text{Double KO}}$ T cell BM chimeras as hosts, where only the T cells are unable to generate SP and HK-1 (Figures S7A–S7C). WT T cell BM chimeras were used as controls. Chimeras with T cells deficient in SP and HK-1 developed a significantly weaker DTH response than that of control T cell BM chimeras (Figures 7H and 7I), a result that correlated with a reduced leukocyte infiltrate at the elicitation site (Figure 7H). In summary, NK1R-signaling by SP and HK-1 released by T cells enhances survival of T cells during priming in secondary lymphoid organs and the effector phase in peripheral tissues.

DISCUSSION

Upon TCR-activation, T cells secrete IL-2 that functions as a T cell growth and differentiation factor. Synthesis and secretion of IL-2 depends in part on activation of Ca^{2+}-dependent transcriptional factors (Ishihara and Schwartz, 2011). Therefore, increase in cytosolic Ca^{2+} is key for activation and survival of T cells (Ganusov et al., 2007). The surge of cytosolic Ca^{2+} after TCR-stimulation relies on activation of PLC-γ1 that hydrolyzes phosphatidylinositol 3, 4-bisphosphate into inositol 1, 4, 5-triphosphate (IP_3), and diacylglycerol (Fracchia et al., 2013). Binding of IP_3 to its receptors on ER membranes releases Ca^{2+} stored within the ER into the cytosol with the subsequent activation of SOCE and entry of extracellular Ca^{2+} (Feske, 2007; Gwack et al., 2007).

A previous study (Stanners et al., 1995) done in membranes isolated from a $G_{\alpha q/11}$-transfected T cell line revealed that generation of optimal concentrations of IP_3 through TCR-stimulation requires physical interaction between the TCR and $G_{\alpha q/11}$ proteins, which results in simultaneous signaling of PLC-γ1 and PLC-β1, respectively. Since then, it has been shown that several GPCR that signal via $G_{\alpha i}$ and $G_{\alpha s}$ or through $G_{\alpha q/11}$ subunits are expressed by T cells on which they exert multiple functions (Bromley et al., 2000; Bueno et al., 2006; Dimitrov et al., 2019; Kremer et al., 2011; Kumar et al., 2006; Liang et al., 2012; Molon et al., 2005; Ngai et al., 2009; Strainic et al., 2008). However, to our knowledge, the identification and *in vivo* relevance of a GPCR that activates and recruits $G_{\alpha q/11}$ proteins to promote optimal levels of intracellular Ca^{2+} in the context of TCR-stimulated T cells have not been described.

Here, we confirmed that both CD4 and CD8 T cells express functional NK1R, a GPCR that together with its high-affinity agonists SP and HK-1 co-segregate at the T cell-DC synapse during cognate activation of T cells. Importantly, our findings that deletion or pharmacological inhibition of the NK1R on T cells cause a significantly decrease in the Ca^{2+} flux triggered by TCR stimulation demonstrate that NK1R signaling is required for optimal Ca^{2+} flux during T cell activation.

The kinetics of intracellular Ca^{2+} increase in T cells following TCR stimulation is bimodal. A transient release of Ca^{2+} from intracellular compartments is followed by a sustained influx of extracellular Ca^{2+} (Gwack et al., 2007; Nohara et al., 2015). In excitable cells, NK1R signaling triggers release of Ca^{2+} from intracellular compartments and intake of extracellular Ca^{2+} (Boyd et al., 1991; Kwatra et al., 1993; Miyano et al., 2010; Mizuta et al., 2008). Likewise, our results demonstrate that NK1R signaling per se increases Ca^{2+} flux in T cells and that NK1R expression enhances intracellular and extracellular Ca^{2+} flux triggered by TCR stimulation. Importantly, the reduction in Ca^{2+} flux we detected in NK1R-deficient T cells after TCR stimulation was not due to an intrinsic impairment of the T cells for Ca^{2+} flux. In fact, $NK1R^{KO}$ and WT T cells exhibited similar kinetics and levels of intracellular Ca^{2+} efflux and extracellular Ca^{2+} influx in response to TCR-independent activation by thapsigargin and ionomycin, respectively.

In our conditions, the increase in Ca^{2+} flux in T cells following NK1R-signaling was reduced by a selective $G_{\alpha q/11}$ protein inhibitor, which indicates that the NK1R recruits $G_{\alpha q/11}$ subunits that likely result in PLC-β1 activation. Likewise, a similar sequence of events has been previously described in non-immune cells signaled via the NK1R (Mizuta et al., 2008; Quartara and Maggi, 1997, 1998).

In excitable cells, stimulation of the NK1R by SP mediates Ca^{2+} influx by increasing the permeability of different voltage-gated channels (Kovac et al., 2006; Rycroft et al., 2007). T cells express different surface Ca^{2+} channels including CRAC, L-type voltage-gated, transient receptor potential channels, and the purinergic P2X receptor (Badou et al., 2013; Gwack et al., 2007). In our experimental conditions, following exhaustion of the intracellular Ca^{2+} stores by thapsigargin, TCR-signaled $NK1R^{KO}$ T cells displayed a significant lower uptake of extracellular Ca^{2+} compared to equally treated WT T cells. These results strongly indicate that in the context of TCR-activation, the NK1R is necessary to activate SOCE.

Besides the high affinity that SP and HK-1 have for the NK1R, recent studies have shown that these tachykinins also bind Mas-related G protein-coupled receptors (Mrgpr), which, similar to the NK1R, recruit $G_{\alpha q/11}$ subunits (Azimi et al., 2016; McNeil et al., 2015; Milligan et al., 2019). These reports might suggest that other GPCR exert the effects described for the NK1R in the present work. However, the substantial decrease in Ca^{2+} flux detected here in T cells lacking functional NK1R demonstrates that indeed the NK1R has a central role in the biologic effects that SP and HK-1 exert in TCR-activated T cells.

In neurons, NK1R-signaling promotes activation of NFAT molecules; however, whether the NK1R exerts a similar effect on immune cells and particularly on TCR-activated T cells was unknown (Quinlan et al., 1999; Seybold et al., 2006; Williams et al., 2007). Here, we show that in the absence of NK1R, a higher number of TCR-activated T cells undergo apoptosis compared to equally stimulated WT T cells and the viability of $NK1R^{KO}$ T cells was significantly improved by supplementation of the culture media with IL-2. Further, we demonstrate that signaling via the NK1R is necessary for calcineurin activation, nuclear translocation of NFAT1, NFAT2, and NF-κB, secretion of IL-2, and surface IL-2Rα expression—which together ultimately result in increased survival of TCR-stimulated T

cells. Our data agree with previous studies that proved that calcineurin activation plays a key role in maintaining high levels of Bcl-2, IL-2, and IL-15, with the consequent increase in activated T cell survival (Manicassamy et al., 2008). Importantly, the absence of the NK1R, did not affect the ability of the surviving T cells to proliferate in response to TCR-signaling, which indicates that NK1R-deficiency does not cause T cell anergy.

A previous study showed that deficiency of the pore subunit Orai1 of the CRAC channels results in diminished influx of extra-cellular Ca^{2+} and nuclear translocation of NFAT, and enhances survival of activated T cells (Kim et al., 2011). The discrepancy in T cell survival between this study and ours could be due to differences in TCR-signaling strength and/or the combined activation of the NFAT and NFκB pathways that follows NK1R signaling, which in our conditions may be necessary for optimal IL-2 secretion by activated T cells (Zambricki et al., 2005).

Besides its function in mature T cells, NK1R-signaling has been shown to be relevant for T cell development in the thymus, which requires activation of PLC-γ1 and Ca^{2+}-dependent NFAT pathways (Fu et al., 2014, 2017; Müller et al., 2009). Indeed, SP sustains proliferation and viability of thymocytes and HK-1 is necessary for maturation of T cell precursors and survival of double-positive thymocytes (Ishihara and Schwartz, 2011; Zhang and Paige, 2003). These observations indicate that NK1R-signaling by its endogenous ligands exerts effects on T cells early during thymic development and at later stages following maturation (Santoni et al., 2002; Zhang and Paige, 2003). Regardless of the effect(s) of NK1R expression during the early stages of thymocyte development, we show here that $NK1R^{KO}$ and WT mature T cells of the spleen express similar levels of TCR, CD3ε, CD4, and CD8, and that following TCR stimulation they exhibit similar kinetics and levels of phosphorylation of ZAP70 and PLC-γ1. Thus, our findings indicate that the reduced Ca^{2+} flux detected in TCR-stimulated $NK1R^{KO}$ T cells is not due to weak or defective TCR downstream signaling.

The role of the Ca^{2+}-dependent NFAT pathway in Th-bias and survival of CD4 T cells has been extensively analyzed (Avni et al., 2002). Mechanistic studies have shown the individual and combined roles of NFAT1 and NFAT2 in Th1- and Th2-polarization through regulation of T-bet and GATA-3, respectively (Di Sabatino et al., 2009; Kiani et al., 2001; Peng et al., 2001; Porter and Clipstone, 2002). In addition, NFAT and TGF-β, which are necessary for differentiation of Th17 and Treg, integrate multiple intracellular signaling to bias naive CD4 T cells to these alternative polarization pathways (Chen et al., 2003; Kim et al., 2014; Oh-Hora et al., 2008; Sundrud and Rao, 2007). Our results show that NK1R-signaling is required for optimal expression of T-bet and RORγt, survival of Th1 cells, and production of IFN-γ by Th1 lymphocytes and IL-17A by Th17 cells. By contrast, lack of the NK1R did not affect the levels of GATA-3, and the subsequent differentiation and survival of Th2 cells. As a result, in the absence of the NK1R, Th1 and Th17 responses are severely compromised as we demonstrated in a Th1- and Th17-mediated model of contact dermatitis in mouse BM chimeras in which T cells, but not other cells, are NK1R-deficient. In agreement with these findings, results from other laboratories and ours, have previously shown that agonistic NK1R-signaling facilitates development of Th1 and Th17 responses in humans and mice (Cunin et al., 2011; Janelsins et al., 2013; Mathers et al., 2007; Nessler et al., 2006; Niizeki

et al., 1999; Reinke et al., 2006; Vilisaar et al., 2015). Thus, NK1R-signaling promotes the type of T cell immunity that sustains chronic inflammatory and autoimmune diseases.

A previous study (Lambrecht et al., 1999) that assessed T cell proliferation *in vitro* by ^{3}H thymidine incorporation concluded that NK1R-signaling augments T cell proliferation induced by CD3 Ab and suboptimal concentration of CD28 Ab. Here, by measuring simultaneously by FACS analysis T cell division by CFSE dilution and T cell viability by fixable viability dye (FVD) exclusion, we demonstrate that under optimal stimulation with CD3 and CD28 Ab, T cells deficient in NK1R or its ligands proliferate and become activated as much as their WT counterparts, but they are unfit to survive.

By using *Tac1*/*4*$^{\text{Double KO}}$ T cells, we show *in vitro* that addition of exogenous HK-1 and SP prevents T cell death, HK-1 exerts a more pronounced effect than SP at equimolar concentrations and they have an additive effect. The additive, rather than a competitive effect, could be ascribed to different molecular stability, receptor affinity, redundancy, or partial agonistic function of the tachykinins (Borbély and Helyes, 2017; Mou et al., 2011; Nederpelt et al., 2016). More research will be necessary to dissect the ultimate molecular mechanism(s) by which SP and HK-1 signal the NK1R on T cells during cognate activation.

In vivo, our findings demonstrate that NK1R-signaling of T cells is necessary during T cell priming and the T cell effector response. In a mouse model of contact dermatitis, T cells deficient in NK1R exhibited increased cell death during Ag-priming in lymph nodes draining hapten-sensitized skin. In an alternative model of contact dermatitis in mouse NK1R$^{\text{KO}}$ T-cell BM chimeras in which T cells are NK1R-deficient, we demonstrate that NK1R-signaling on T cells enhances survival of effector T cells at the elicitation site and is required for development of an optimal cutaneous DTH in response to the hapten.

Using *in vitro* models, previous studies (Lambrecht et al., 1999; Zhang and Paige, 2003) have suggested that the effects of SP and HK-1 on T cells are likely due to autocrine secretion of these NK1R agonists. Similarly, our *in vitro* assays of TCR stimulation with Ab, done exclusively with purified WT or NK1R$^{\text{KO}}$ T cells and without exogenous NK1R ligands, indicated that the T cells themselves release NK1R agonists. Indeed, we confirmed the presence of *Tac1* and *Tac4* mRNA in resting and TCR-stimulated T cells and by ImageStream, we detected SP and HK-1 peptides generated by WT T cells cognately stimulated by *Tac1*/*4*$^{\text{Double KO}}$ DCs.

In vivo, sensory neurons and leukocytes other than T cells can be alternative sources of SP and HK-1 (Santoni et al., 1999; Steinhoff et al., 2014). Here, we show that *Tac1*/*4*$^{\text{Double KO}}$ T cell BM mouse chimeras developed substantially reduced skin contact hypersensitivity. These results strongly indicate that SP and HK-1 released by T cells act in an autocrine/paracrine fashion. Whether other cellular sources of SP or HK-1 contribute to prevent T cell death during cognate activation requires further research and is beyond the scope of this study.

In summary, we demonstrate that NK1R-signaling of T cells enhances Ca^{2+} flux in T cells after TCR-signaling and that this effect is mediated by autocrine/paracrine secretion of SP and HK-1. This effect is necessary for the subsequent downstream pathways that initiate

IL-2 synthesis, T cell survival, and Th1- and Th17-polarization. In a model of contact dermatitis, NK1R-signaling increased survival of T cells during priming in secondary lymphoid tissues and of effector T cells in peripheral tissues. Consequently, mice with T cells deficient in NK1R or its agonists developed poor contact hypersensitivity responses to the hapten. Our results reveal a fundamental and previously unknown role for the NK1R and its agonists in T cell biology, which is relevant for the development of stimulatory or suppressive immunotherapies.

STAR★METHODS

LEAD CONTACT AND MATERIALS AVAILABILITY

Further information and requests for resources should be directed to and will be fulfilled by the Lead Contact, Adriana T. Larregina (adrianal@pitt.edu). This study did not generate new models or unique reagents.

EXPERIMENTAL MODEL AND SUBJECT DETAILS

Mice—Seven week-old male or female C57BL/6(B6), B6.SJL-Ptprc^{a}Pepc^{b}/BoyJ (CD45.1), B6.PL-Thy1^{a}/CyJ (Thy1.1), B6.129S2-Tcra^{tm1Mom}/J (TcRαβ^{KO}) and B6.Cg-Tg(TcraTcrb) 425Cbn/J (OT-II) mice were purchased from The Jackson Laboratory. Homozygous NK1R^{KO} and *Tac1*/*4*$^{Double\ KO}$ B6 mice, generated and provided by A. Berger and C.J. Paige (University of Toronto, Canada) (Berger et al., 2010, 2012), were bred in the animal facility of the University of Pittsburgh School of Medicine. Seven to 12-week old male or female mice were randomly selected for the experiments in accordance to the National Institutes of Health scientific rigor policy. Mice were maintained in the pathogen free animal facility of the University of Pittsburgh School of Medicine that provides with around the clock husbandry and veterinary services. Animal care and handling were performed in accordance to institutional guidelines and the procedures approved by IACUC protocol number 19014279.

Generation of DC and T cell purification—Bone marrow (BM)-derived dendritic cells (DC) (BMDC) were generated by culturing BM precursor cells isolated from tibias and femurs of WT, NK1R^{KO} or *Tac1*/*4*$^{Double\ KO}$ B6 mice. BM cells were cultured in RPMI-1640 culture medium with 10% FBS, mouse GM-CSF (1000 U/ml), and mouse IL-4 (500 U/ml). On day 6, BMDC were purified by positive selection with mouse CD11c MicroBeads (Miltenyi) (CD11c^{+} BMDC purity > 90%). T cells were isolated from spleens of WT, NK1R^{KO}, *Tac1*/*4*$^{Double\ KO}$ and OTII mice and purified by negative selection with Dynabeads Untouched Mouse Total T cell, CD4 T cell or CD8 T cell kits (Invitrogen). CD4 regulatory T cells were depleted by adding CD25 Ab (clone PC61.5) to the Ab cocktail mix of the negative selection kits.

METHOD DETAILS

Detection of the NK1R by flow cytometry—For labeling of surface NK1R, purified WT or NK1R^{KO} T cells were incubated with an Ab against the extracellular domain of the mouse / rat / human NK1R and ATTO-488-conjugated (Alomone Laboratories), in combination with APC-CD4 Ab and V500-CD8α Ab (1:100, 30 min on ice). For labeling of

the intracellular (C terminus) domain of the NK1R, T cells were first incubated with APC-CD4 Ab and V500-CD8α Ab (1:100, 30 min, on ice). Next, T cells were washed in ice-cold PBS, fixed in 2% paraformaldehyde (15 min, RT), and permeabilized with 0.1% saponin 1% FBS in PBS (10 min, RT). Permeabilized cells were incubated with an Ab recognizing the intracellular domain (C terminus) of the mouse / rat / human NK1R and PE-conjugated (Santa Cruz) (1:200, 30 min, 4°C). Cell were washed in permeabilization buffer and in PBS, and immediately analyzed with a BD LSR II flow cytometer. Results were analyzed with the FlowJo v10 software. Fluorochrome-conjugated species and isotype Ig irrelevant Ab were used as staining controls.

ImageStream® analysis—WT, NK1R^{KO} and *Tac1/4*$^{Double\ KO}$ B6 BMDC were purified with mouse CD11c MicroBeads (Miltenyi). Purified OT-II CD4 T cells were labeled with Cell Tracker Violet (Thermo Fisher). WT, NK1R^{KO} and *Tac1/4*$^{Double\ KO}$ B6 BMDC were left untreated or loaded with 1 μM of $OVA_{323–339}$ peptide (1 h, 37°C), washed in PBS, and then incubated with the Cell Tracker Violet-labeled OT-II cells (1 DC: 1 T cell, 10^6 of each cell) in 1 mL polypropylene tubes, for 2 h, at 37°C. Next, cells were transferred to 1.5 mL Eppendorf tubes and washed with ice-cold 5% FBS / PBS without EDTA. All centrifugations were done in a refrigerated centrifuge (200 *g*, 4 min, 4°C). Cells were surface labeled with APCCy7-CD11c Ab (1:100) and ATTO488-NK1R Ab against the extracellular domain of the NK1R (Alomone Labs,1:100), washed with ice-cold 5% FBS / PBS without EDTA, and fixed with 1.5% paraformaldehyde (30 min, RT). Next, cells were washed to remove the fixative with ice-cold 5% FBS / PBS without EDTA, permeabilized with 100 μl of 0.1% Triton-X (Sigma), and labeled intracellularly with (i) Cy3-SP Ab (Bioss USA, 1:100), AF647-HK-1 Ab (Peninsula Laboratories, 1:50), and Texas redphalloidin (1:50); or (ii) rhodamine-phalloidin (1:50). Cells were washed with ice-cold PBS without EDTA, fixed with 1.5% paraformaldehyde and read immediately, or left in ice-cold PBS without EDTA until analysis. Appropriate species and isotype Ig irrelevant Ab were used as controls. Five thousand cells were collected with a two-laser Amnis ImageStream® analyzer, at a magnification X60. Cell images were analyzed with the software IDEAS v6.2.

Ca^{2+} flux assays—For ratiometric analysis of Ca^{2+} flux by FACS, purified T cells were incubated with APC-CD4 Ab, Pacific blue-CD8α Ab and Fixable Viability Dye eFluor 780 (30 min, on ice). After washing in PBS, T cells were resuspended in PBS without Ca^{2+} and Mg^{2+} and loaded with Fluo-4-AM and Fura Red- AM Cell Permeant (2uM each) (30 min, in the dark, 37°C). After thoroughly washing in PBS without Ca^{2+} and Mg^{2+}, 2×10^6 T cells were resuspended in 1 mL of PBS containing 25 mM HEPES 0.9 mM Ca^{2+} 0.5 mM Mg^{2+} and 1 mM sodium pyruvate, and incubated with hamster anti-mouse CD3ε agonistic Ab (clone 145–2C11, 1 μg / ml) for 30 min on ice. Five min prior to recording, the FACS tubes containing the T cells were placed in a water bath at 37°C, a temperature that was maintained throughout the recording time. Cells were analyzed immediately with BD LSR II or Fortessa flow cytometers. Each sample was recorded for 30 s (baseline) prior to addition of (SarSP) or anti-hamster IgG (10 μg/ml) to crosslink the CD3ε Ab. In some experiments, T cells incubated with CD3ε Ab were treated with the NK1R antagonists L733,060 or WIN 51708 (both at 10^{-5} M, for 20 min, 37°C) prior to recording of the baseline and addition of the anti-hamster IgG.

To assess Ca^{2+} efflux from the intracellular compartment, T cells were incubated with CD3ε Ab and kept in ice-cold PBS without Ca^{2+} and Mg^{2+}. Five min before recording, the FACS tubes containing the T cells were placed in a water bath at 37°C and the temperature kept during the recording time. After recording the 30 s baseline, T cells were treated anti-hamster IgG to initiate CD3ε Ab crosslinking and data were recorded for 4 min.

For analysis of SOCE activation, T cells were incubated with CD3ε Ab and maintained in ice-cold PBS without Ca^{2+} and Mg^{2+}. Five min prior to recording, the FACS tubes with the T cells were placed in a water bath at 37°C and the temperature maintained during the recording time. After recording the 30 s baseline, T cells were treated with thapsigargin (0.5 μM) and efflux of Ca^{2+} from the intracellular compartment recorded for 4 min. Next, Ca^{2+} (20 mM) and anti-hamster IgG were added and influx of extracellular Ca^{2+} was recorded during the following 3 min. As positive controls, T cells were stimulated with ionomycin (1 μM) after recording the 30 s baseline. Negative controls included T cells non-treated or incubated with CD3ε Ab alone without crosslinking, in which data were recorded for 5 min. In all cases, T cell viability was assessed by FVD exclusion at the end of the Ca^{2+} flux assay.

The ratiometric Fluo-4-AM / Fura Red AM analysis was performed using the derived parameter of the FlowJo v10 software and the kinetics tool was used to represent the Ca^{2+} flux graphically. Statistical comparison of Ca^{2+} flux from independent samples was achieved by comparing the area under the curve (AUC) per variable with the kinetics analysis function of the FlowJo v10 software.

For analysis of Ca^{2+} flux by live-cell microscopy, purified CD4 T cells were loaded with Fluo-4-AM as described above, and kept in PBS with 1 mM sodium pyruvate, 25 mM HEPES, 0.9 mM Ca^{2+} and 0.5 mM Mg^{2+}, at 37°C. Next, T cells were placed on poly-L-lysine coated glass bottom cell culture dishes (30 mm diameter, MatTek) at 1.5×10^5 T cells per dish and allowed to settle down for 10 min before imaging. T cells were imaged using a Nikon Ti inverted microscope equipped with a 1.40 N.A 60x objective and Photometrics Prime 95B sCMOS camera. Basal fluorescence intensity was obtained by imaging unstimulated cells for 80 s. Next, cells were stimulated by either SarSP (10^{-7} M) alone or with the $G_{\alpha q/11}$ inhibitor YM 254,890 (10 μM). Cells were imaged once per sec using a Lumencore Spectra X LED excitation source. The total imaging period for each variable was 10 min. Images and fluorescence intensity of each cell was analyzed with the NIS Elements v5.11.01 (Nikon Instruments Inc). Quantification of Ca^{2+} flux on each individual cell was calculated by the difference between the maximal and minimal Fluo-4 AM fluorescence signal intensity (peak value). Representative figures were generated by selecting single cells whose Ca^{2+} flux intensity profile fell within 2 standard deviations of the mean for each group.

Western blot analysis—For detection of the f-NK1R and t-NK1R variants in resting and activated T cells, purified CD4 T and CD8 T cells were left untreated or cultured in 24 well plates (4×10^6 cells per well) in RPMI 1640 medium supplemented with 10% FBS, and incubated with plate-bound CD3ε Ab (145–2C11, 5 μg / ml) plus soluble CD28 Ab (37.51, 10 μg / ml), for 24 h. Total protein was isolated with RIPA buffer in the presence of Protease Inhibition Cocktail (Sigma). Protein (40 μg) with Laemmli sample buffer was resolved on

Any kD Mini-PROTEAN® TGX Precast Protein Gels (BIO-RAD). After transfer, PVDF membranes (BIO-RAD) were blocked with Odyssey Blocking Buffer (LI-COR), then probed with anti-mouse NK1R N terminus Ab (Novus Biological) and anti-mouse NK1R C terminus Ab (Clone D-11, Santa Cruz).

For detection of basal levels of ZAP70 and PLC-γ1 in WT or $NK1R^{KO}$ T cells, protein from purified total T cells was extracted with RIPA buffer containing Protease Inhibition Cocktail. Protein was quantified using the Pierce® BCA Protein Assay. Samples were diluted in 4x Laemmli sample buffer with DTT and incubated on a heating block (95°C, 5 min). Protein (20 μg) was resolved on Any kD Mini-PROTEAN® TGX Precast Protein Gels and transferred to PVDF membranes that were blocked with Odyssey Blocking Buffer. Membranes were probed with anti-PLC-γ1 Ab (1:1000), anti-ZAP70 Ab (1:1000), and anti-GAPDH Ab (1:5000).

For detection of nuclear translocation of transcription factors, purified total WT or $NK1R^{KO}$ T cells were incubated in 24-well plates (2×10^6 T cells / well) alone for 120 min (mock), or with plate-bound CD3ε Ab (145–2C11, 5 μg / ml) plus soluble CD28 Ab (37.51, 10 μg / ml) for 30, 60, 120 or 240 min, or with ionomycin (1 μM) for 120 min, all at 37°C. After incubation, cytoplasmic and nuclear protein extracts were prepared on fresh pellets with the NE-PER nuclear and cytoplasmic extraction reagent and quantified using the Pierce® BCA Protein Assay (both from Thermo Scientific). Next, samples were diluted in 4x Laemmli sample buffer with DTT, incubated on a heating block (95°C, 5 min), and 10 μg of protein loaded in Any kD Mini-PROTEAN® TGX Precast Protein Gels. Gels were electroblotted on PVDF membranes. Blots were blocked (1 h, room temperature) with Odyssey Blocking Buffer before probing in the following combinations of primary Ab (overnight, 4°C): (i) rabbit anti-NFAT2 Ab (1:1000) plus goat anti-cFos Ab (1:200); (ii) rabbit anti-NFAT1 Ab (1:1000) plus goat anti-cJun Ab (1:200); and (iii) goat anti-NFκβ-p65 Ab (1:200). Rabbit anti-TBP Ab (1:2000) or mouse anti-GAPDH Ab (1:5000), were used to assess equal loading of nuclear and cytoplasmic extracts, respectively.

In all cases, membranes were incubated (1 h, room temperature) with the appropriate secondary Ab conjugated with IRDye® 680 or 800 (LI-COR) or DyLight 800 (Thermo Fisher) and scanned on the Odyssey Imaging System (LI-COR). The intensity of the signal was quantified with the Image Studio software v2 and the ImageJ software version 1.51 s (LI-COR).

Detection of phosphorylated ZAP70/Syk and PLC-γ1 by flow cytometry—

Purified WT and $NK1R^{KO}$ T cells (5×10^6) were incubated with CD3ε Ab (clone 145–2C11, 1 μg/ml, 30 min, 4°C) and equilibrated at 37°C in a water-bath for 10 min before adding anti-hamster IgG (10 μg/ml) to crosslink the CD3ε Ab and initiate TCR-signaling. After 1, 5, 10 or 20 min, T cell activation was stopped by adding 100 μL of 34% formaldehyde into the 1 mL final volume of the sample, and T cells were fixed for 10 min. Next, cells were washed in PBS, permeabilized with ice-cold methanol (15 min, RT), washed in PBS, and resuspended in 200 μL PBS. Permeabilized T cells were incubated with APC-CD4 Ab, FITC-CD8α Ab, and anti-mouse / human phospho ZAP70 (Tyr_{319}) / phospho Syk (Tyr_{352}) Ab PE-conjugated (clone E267, 1:100, 20 min, RT), or anti-mouse /

human phosphor PLC-γ1 (Tyr_{783}) (clone PLCGTYR783-C4, 1:100, 20 min, RT). After washing in PBS, samples were immediately analyzed by FACS.

Measurement of NFAT nuclear translocation by flow cytometry—Detection of nuclear translocation of NFAT1 and NFAT2 in T cells by FACS was done as described in Carretta et al. (2018). Briefly, purified WT or $NK1R^{KO}$ T cells were incubated in 24-well plates (3×10^6 T cells / well) alone for 120 min (mock), or with plate-bound CD3ε Ab (145–2C11, 5 μg / ml) plus soluble CD28 Ab (37.51, 10 μg / ml) for 30, 60, 120 or 240 min, or with ionomycin (1 μM) for 120 min, all at 37°C. At each endpoint, T cells were collected, washed in ice-cold 1% FBS – PBS and centrifuged (500*g*, 4°C, 5 min). For cell nuclei isolation, T cell pellets were resuspended in 600 μl of ice-cold Pipes-Triton buffer [10 mM free acid Pipes, 0.1M NaCl, 2mM $MgCl_2$, 0.1% Triton X-100, 1 mM DTT, Halt Protease Inhibitor Cocktail (1:100, Thermo Scientific), in sterile dd water, pH 6.8], vortexed for 10 s, transferred to FACS tubes, and incubated on ice. After 30 min, cell nuclei were centrifuged (500*g*, 10 min, 4°C), the supernatants were removed carefully, and the pellets resuspended in 200 μl of ice-cold 1% BSA – PBS buffer and gently pipetted up and down 3–5 times with a p-1000 pipettor. T cell nuclei were incubated with AF488-NFAT1 Ab (1:50) (Cell Signaling), AF488-NFAT2 Ab (1:100) (BioLegend), or AF488-conjugated species and isotype Ig irrelevant Ab as staining controls (30 min, on ice). Next, T cell nuclei were washed with ice-cold 1% BSA – PBS buffer, incubated with propidium iodide (1:50, 5 min, on ice), washed in ice-cold 1% BSA – PBS buffer, and fixed in 2% paraformaldehyde. Data were acquired with a BD LSR II flow cytometer and analyzed using FlowJo v10 software.

For visualization of T cell nuclei purity and integrity, T cell nuclei were centrifuged (300 rpm, 5 min) with a Cytospin 3 centrifuge (Shandon) on poly-L-lysine coated slides. Cytospins were fixed with 1% paraformaldehyde (10 min, RT), rinsed in PBS, permeabilized with 0.3% Triton X-100 – PBS (15 min, RT), rinsed in PBS, and incubated with fluorescein-phalloidin (1:500) and propidium iodide (1:50), for 15 min at RT. Cytospins were rinsed in PBS, fixed in 2% paraformaldehyde and examined with a Nikon Eclipse E800 microscope equipped with a CCD camera.

Analysis of T cell proliferation, activation and cell death—Purified T cells from spleens of WT, $NK1R^{KO}$ or *Tac1/4*$^{\text{Double KO}}$ B6 were labeled with CFSE (1 μM) and then cultured in RPMI 1640 medium with 10% FBS (10^6 T cells per 2 mL of medium per well), in 24 well plates, in the presence of plate-bound CD3ε Ab (145–2C11, 5μg / ml) plus soluble CD28 Ab (37.51, 10 μg / ml) alone, or with SP (10^{-9} M), HK-1 (10^{-8} M), or both, added on days 1 and 3 of culture. In some experiments, human IL-2 (50 U / ml) was added at the start of the cultures. After 4 days, cells were labeled with BUV395-CD4, PECy5-CD8 and PE-CD44 Ab, plus eFluor® 780-Fixable Viability Dye (FVD) (eBioscience).

For analysis of T cell death, CFSE-labeled purified WT or $NK1R^{KO}$ T cells were cultured in RPMI 1640 medium with 10% FBS (10^6 T cells per 2 mL of medium per well), in 24 well plates, in the presence of plate-bound CD3ε Ab (145–2C11, 5μg / ml) plus soluble CD28 Ab (37.51, 10 μg / ml) alone, or with the necroptosis inhibitor Necrostatin-1 (2 μg/ml, Sigma) or equivalent concentration of its vehicle, DMSO. After 4 days, cells were incubated with PE-Annexin V, 7AAD, NucView® 405 Caspase-3 Substrate (1:1000, Biotium), BUV395-CD4

Ab, APC-CD8 Ab, PE-Cy7-CD3ε Ab, and eFluor® 780-FVD, and immediately analyzed by FACS without fixation. In all experiments, appropriate irrelevant Abs were used as controls and, unless stated, cells were fixed in 4% paraformaldehyde – PBS. Data were acquired with BD LSR II or Fortessa flow cytometers and analyzed using FlowJo v10 software.

Generation of polarized T cells—Naive CD4 T cells were isolated from spleens of WT and NK1R^{KO} B6 mice. First, erythrocytes were removed by incubation with red blood cell lysis buffer. Next, splenocytes were incubated with CD19 Ab followed by sheep anti-rat IgG Dynabeads and B cells were depleted by magnetic sorting. B cell-depleted splenocytes were incubated with the following Ab: (i) FITC-conjugated NK1.1, CD11b, B220, CD8β, and CD25 Ab (lineage cocktail); (ii) PE-CD62L Ab; (iii) APC-CD4 Ab; and (iv) E450-CD44 Ab. Lineage^{neg} CD4^{+} CD62L^{hi} CD44^{lo} cells (naive CD4 T cells) were sorted with a BD-FACSAria flow cytometer (naive CD4 T cell purity > 94%). WT or NK1R^{KO} naive CD4 T cells were labeled with CFSE (1 μM), and cultured (10^6 cells in 2 mL of medium per well, 24-well plates) in RPMI 1640 medium containing 10% FBS and artificial APC (Dynabeads Mouse T-Activator CD3/CD28 For T cell Expansion and Activation) at 1 bead: 1 T cell ratio, for Th1, Th2 and Th17 polarization. To promote polarization of CD4 T cells, cultures were supplemented with the following reagents: (i) for Th1-polarization, IL-12p70 (10 ng / ml) plus IL-4 Ab (10 μg / ml); (ii) for Th2-bias, IL-4 (10 ng / ml) plus IFN-γ Ab (10 μg / ml); and (iii) for Th17-polarization, IL-6 (20 ng / ml), TGF-β1 (5ng / ml), IL-23 (10 ng / ml), IL-4 Ab (10 μg / ml), and IFN-γ Ab (10 μg / ml). After 4 days of culture, T cells were stimulated with PMA (50 ng / ml) and ionomycin (0.7 μM) in the presence of brefeldin A (BD GolgiPlug), for 5 h at 37°C. Cells were surface stained with APC-CD4 Ab in combination with eFluor® 780-FVD, then fixed with 2% paraformaldehyde, permeabilized with 0.1% saponin / 1% FBS / PBS solution, and labeled intracellularly with PE-IL-4, PerCPCy5.5-IFN-γ, and BUV395-IL-17A Ab. Alternatively, cells were surface labeled with APC-CD4 Ab plus eFluor® 780-FVD, then fixed in paraformaldehyde, permeabilized with eBioscience Foxp3 / Transcription Factor Staining Buffer, and labeled intracellularly with PE-T-bet, PE-GATA-3, or PE-RoRγt. Appropriate fluorochrome-conjugated irrelevant Ab were used as controls. Cells were analyzed with a BD LSR II or Fortessa flow cytometers and analyzed using FlowJo v10 software.

Analysis of Ag (hapten)-specific T cells in skin-draining lymph nodes—Purified T cells from spleens of WT (CD45.2 Thy1.1) and NK1R^{KO} (CD45.2 Thy1.2) mice were CFSE (1 μM)-labeled and i.v. injected (20×10^6 of each T cell subset per mouse) in host WT (CD45.1) B6 mice. After 24 h, mice were sensitized with 2 doses of DNCB (0.5% in 4:1 acetone / olive oil) applied 24 h apart on the shaved lower abdominal skin. Mice were euthanized on day 5 after T- cell transfer and the skin-draining lymph nodes (inguinal) were dissected. Single cell suspensions of the lymph nodes were labeled with APC-CD3, V450-CD4, V500-CD8, PE-CD44, FITC-CD45.2, PECy5-CD45.1, BUV395-Thy1.1, and PECy7-Thy1.2 Ab in combination with eFluor® 780-FVD and analyzed by FACS.

ELISA and ELISA-based assays—Concentrations of IL-2 in 24 h culture supernatants of WT, NK1R^{KO}, *Tac1/4*$^{\text{Double KO}}$ CD4 or CD8 T cells cultured alone or in the presence of plate-bound CD3ε Ab (145–2C11, 5μg / ml) and soluble CD28 (37.51, 10μg / ml) Ab, with

or without SP or HK-1 (both at 10^{-9} M), were measured by ELISA (R&D). Quantification of calcineurin activity was assessed with the colorimetric Calcineurin Cellular Activity Assay Kit (EMD Millipore). Concentrations of IFN-γ, IL-2, IL-5, IL-13, and IL-17A in 4-day culture supernatants of polarized CD4 T cells were assessed by ELISA (BD, Thermo Fisher).

Real time quantitative PCR (RT-qPCR)—RNA was extracted with TRIzol Reagent (Thermo-Fisher Scientific) from purified WT CD4 T and CD8 T cells untreated or following 2, 4, 6 or 24 h stimulation with CD3 Ab and CD28 Ab as described above. RNA was reverse transcribed to cDNA using the iScript™ Reverse Transcription Supermix for RT-qPCR (Bio-Rad). Pre-designed primers for detection of cDNA transcribed from *PPT-A* mRNA (*TAC1*) and *PPT-C* mRNA (*TAC4*) were from SABioscience (QIAGEN). Primers (250 mM) were mixed with 10 μL of 2X Fast SYBR Green Master Mix (Thermo Fisher), 2 ul of cDNA, and brought to a final volume of 20 μL with DNAase-/RNAase-free water. The PCR cycling conditions were as follows: initial hold for 20 s at 95°C (polymerase activation), 40 cycles at 95°C for 3 s (denature) and 60°C for 15 s (annealing/extending). Gene expression was normalized to GAPDH to control for RNA integrity and loading, and to compensate for inter-PCR variations using the $2^{-\Delta\Delta Ct}$ method. PCR was done in a StepOnePlus Real-Time PCR System (Applied Biosystems).

Generation of NK1R^{KO} and Tac1/4$^{Double\ KO}$ BM T cell chimeras—Male TCRαβ^{KO} B6 mice (5–6-week old) were γ-irradiated with 550 rads twice, 6 h apart. Two h later, the irradiated TCRαβ^{KO} B6 mice were i.v. injected with male 10^7 BM cells. For production of the NK1R^{KO} T cell BM chimeras, the BM inoculum contained 80% BM cells from TCRαβ^{KO} B6 mice plus 20% BM cells from NK1R^{KO} B6 mice. For generation of *Tac1/4*$^{Double\ KO}$ T cell BM chimeras, hosts were infused with 80% BM cells from TCRαβ^{KO} B6 mice and 20% BM cells from *Tac1/4*$^{Double\ KO}$ B6 mice. For generation of control WT T cell BM chimeras, host mice were injected with 80% BM cells from TCRαβ^{KO} B6 mice and 20% BM cells from WT B6 mice. Animals were kept in autoclaved cages, provided with sterile water with Sulfatrim during the first week, and full-developed chimeras were used 8 weeks after BM infusion.

The absence of the NK1R, *Tac1* or *Tac4* WT alleles in T cells and their presence in the non-T cell leukocyte lineages were tested by genomic PCR on αβ T cells and non-αβ T cell leukocytes FACS-sorted from spleens of the BM chimeras. PCR was performed as described in Berger et al. (2010, 2012). The percentages of leukocytes subpopulations in the experimental and control chimeras were analyzed by FACS on splenocytes labeled with the following combinations of fluorochrome-conjugated Ab: (i) APC-CD3, BUV395-CD4, V500-CD8, PE-CD44 and PE-Cy5-CD62L; and (ii) APC-CD3, BUV395-CD4, PE-FoxP3 and FITC-CD19.

Induction of contact dermatitis and assessment of skin-homed T cells—NK1R^{KO} T cell, *Tac1/4*$^{Double\ KO}$ T cell, and control WT T cell BM chimeras were sensitized once with DNCB (0.5% in 4:1 acetone / olive oil) or vehicle on the shaved abdominal skin. After 5 days, mice were challenged with DNCB (0.5% in 4:1 acetone / olive oil) on the dorsal side of the right ear and with vehicle on the left ear (control). Ear thickness increase

was measured with a caliper at successive days after Ag challenge. In some experiments, mice were euthanized 48 h after challenge and the ears were dissected, fixed in 4% paraformaldehyde, embedded in paraffin, sectioned and stained with hematoxylin and eosin. Alternatively, ear skin fragments were snap-frozen, and 10 μm cryosections were placed on Vectabond Reagent (Vector)-treated slides, fixed with 4% paraformaldehyde (15 min, room temperature), blocked with 5% goat serum and the avidin/biotin blocking kit (Vector), and incubated with biotin-CD3 Ab plus DyLight 488-streptavidin, followed by labeling with the *In Situ* Cell Death Detection kit, TMR red (Roche). For negative controls, the biotin-CD3 Ab was replaced by biotin-Armenian hamster irrelevant IgG followed by Cy2-streptavidin. Cell nuclei were stained with 4′6-diamidino-2-phenylindole 2HCl (DAPI) (Thermo Fisher). Skin sections were analyzed with a Zeiss Axiovert 135 microscope equipped with a CCD camera (Photometrics CH 250). Identification and quantification of infiltrating leukocytes at the site of skin DNCB elicitation was done on single cell suspensions obtained by digestion of ear skin fragments as described in Mathers et al. (2007). Cells were then labeled with FITC-CD45, BUV395-CD4 and PECy5-CD8 Ab, and analyzed by FACS.

QUANTIFICATION AND STATISTICAL ANALYSIS

Statistical analysis was performed using the GraphPad Prism v7 software (San Diego, CA) Results are expressed as mean ± 1SD. Comparisons of two means were done by two-tailed Student's t test. Comparison of multiple means on a single dataset were done by ANOVA followed by *ad hoc* Student Newman Keuls test. A "p" value < 0.05 was considered significant.

DATA AND CODE AVAILABILITY

This study did not generate any unique datasets or code.

Supplementary Material

Refer to Web version on PubMed Central for supplementary material.

ACKNOWLEDGMENTS

This work was supported by the NIH grants R01AR068249 and R01AR071277 (to L.D.F. and A.T.L.), R01AR074285 (to L.D.F.), R01HL130191 and R01AI148690 (to A.E.M.), and K01AR067250 (to T.L.S.); The Thomas E. Starzl Postdoctoral Fellowship in Transplantation Biology (to D.M.R.-C.); and the National Cancer Institute of Canada Terry Fox Program Project Grant 015005 and the Canadian Institute of Health Research grant 9862 (to A.B. and C.J.P.).

REFERENCES

Avni O, Lee D, Macian F, Szabo SJ, Glimcher LH, and Rao A (2002). T(H) cell differentiation is accompanied by dynamic changes in histone acetylation of cytokine genes. Nat. Immunol 3, 643–651. [PubMed: 12055628]

Azimi E, Reddy VB, Shade KC, Anthony RM, Talbot S, Pereira PJS, and Lerner EA (2016). Dual action of neurokinin-1 antagonists on Mas-related GPCRs. JCI Insight 1, e89362. [PubMed: 27734033]

Badou A, Jha MK, Matza D, and Flavell RA (2013). Emerging roles of L-type voltage-gated and other calcium channels in T lymphocytes. Front. Immunol 4, 243. [PubMed: 24009608]

Benvenuti F (2016). The dendritic cell synapse: a life dedicated to T cell activation. Front. Immunol 7, 70. [PubMed: 27014259]

Berger A, and Paige CJ (2005). Hemokinin-1 has substance P-like function in U-251 MG astrocytoma cells: a pharmacological and functional study. J. Neuroimmunol 164, 48–56. [PubMed: 15913794]

Berger A, Benveniste P, Corfe SA, Tran AH, Barbara M, Wakeham A, Mak TW, Iscove NN, and Paige CJ (2010). Targeted deletion of the tachykinin 4 gene (TAC4−/−) influences the early stages of B lymphocyte development. Blood 116, 3792–3801. [PubMed: 20660792]

Berger A, Tran AH, Dida J, Minkin S, Gerard NP, Yeomans J, and Paige CJ (2012). Diminished pheromone-induced sexual behavior in neurokinin-1 receptor deficient (TACR1(−/−)) mice. Genes Brain Behav. 11, 568–576. [PubMed: 22471406]

Borbély É, and Helyes Z (2017). Role of hemokinin-1 in health and disease. Neuropeptides 64, 9–17. [PubMed: 27993375]

Boyd ND, MacDonald SG, Kage R, Luber-Narod J, and Leeman SE (1991). Substance P receptor. Biochemical characterization and interactions with G proteins. Ann. N Y Acad. Sci 632, 79–93. [PubMed: 1659301]

Bozic CR, Lu B, Höpken UE, Gerard C, and Gerard NP (1996). Neurogenic amplification of immune complex inflammation. Science 273, 1722–1725. [PubMed: 8781237]

Bromley SK, Peterson DA, Gunn MD, and Dustin ML (2000). Cutting edge: hierarchy of chemokine receptor and TCR signals regulating T cell migration and proliferation. J. Immunol 165, 15–19. [PubMed: 10861029]

Bueno C, Lemke CD, Criado G, Baroja ML, Ferguson SS, Rahman AK, Tsoukas CD, McCormick JK, and Madrenas J (2006). Bacterial superantigens bypass Lck-dependent T cell receptor signaling by activating a Galpha11-dependent, PLC-beta-mediated pathway. Immunity 25, 67–78. [PubMed: 16860758]

Carretta MD, Hidalgo MA, and Burgos RA (2018). Indirect measurement of CRAC channel activity using NFAT nuclear translocation by flow cytometry in Jurkat cells. Methods Mol. Biol 1843, 83–94. [PubMed: 30203279]

Chen CH, Seguin-Devaux C, Burke NA, Oriss TB, Watkins SC, Clipstone N, and Ray A (2003). Transforming growth factor beta blocks Tec kinase phosphorylation, Ca^{2+} influx, and NFATc translocation causing inhibition of T cell differentiation. J. Exp. Med 197, 1689–1699. [PubMed: 12810687]

Cunin P, Caillon A, Corvaisier M, Garo E, Scotet M, Blanchard S, Delneste Y, and Jeannin P (2011). The tachykinins substance P and hemokinin-1 favor the generation of human memory Th17 cells by inducing IL-1β, IL-23, and TNF-like 1A expression by monocytes. J. Immunol 186, 4175–4182. [PubMed: 21368235]

Dimitrov S, Lange T, Gouttefangeas C, Jensen ATR, Szczepanski M, Lehnnolz J, Soekadar S, Rammensee HG, Born J, and Besedovsky L (2019). Ga_s-coupled receptor signaling and sleep regulate integrin activation of human antigen-specific T cells. J. Exp. Med 216, 517–526. [PubMed: 30755455]

Di Sabatino A, Rovedatti L, Kaur R, Spencer JP, Brown JT, Morisset VD, Biancheri P, Leakey NA, Wilde JI, Scott L, et al. (2009). Targeting gut T cell Ca^{2+} release-activated Ca^{2+} channels inhibits T cell cytokine production and T-box transcription factor T-bet in inflammatory bowel disease. J. Immunol 183, 3454–3462. [PubMed: 19648266]

Endo T, Yanagawa Y, and Komatsu Y (2016). Substance P activates Ca^{2+-} permeable nonselective cation channels through a phosphatidylcholinespecific phospholipase C signaling pathway in nNOS-expressing GABAergic neurons in visual cortex. Cereb. Cortex 26, 669–682. [PubMed: 25316339]

Feske S (2007). Calcium signalling in lymphocyte activation and disease. Nat. Rev. Immunol 7, 690–702. [PubMed: 17703229]

Fracchia KM, Pai CY, and Walsh CM (2013). Modulation of T cell metabolism and function through calcium signaling. Front. Immunol 4, 324. [PubMed: 24133495]

Fu G, Rybakin V, Brzostek J, Paster W, Acuto O, and Gascoigne NR (2014). Fine-tuning T cell receptor signaling to control T cell development. Trends Immunol. 35, 311–318. [PubMed: 24951034]

Fu G, Yu M, Chen Y, Zheng Y, Zhu W, Newman DK, Wang D, and Wen R (2017). Phospholipase Cγ1 is required for pre-TCR signal transduction and pre-T cell development. Eur. J. Immunol 47, 74–83. [PubMed: 27759161]

Ganusov VV, Milutinović D, and De Boer RJ (2007). IL-2 regulates expansion of CD4+ T cell populations by affecting cell death: insights from modeling CFSE data. J. Immunol 179, 950–957. [PubMed: 17617586]

Ge C, Huang H, Huang F, Yang T, Zhang T, Wu H, Zhou H, Chen Q, Shi Y, Sun Y, et al. (2019). Neurokinin-1 receptor is an effective target for treating leukemia by inducing oxidative stress through mitochondrial calcium overload. Proc. Natl. Acad. Sci. USA 116, 19635–19645. [PubMed: 31488714]

Grakoui A, Bromley SK, Sumen C, Davis MM, Shaw AS, Allen PM, and Dustin ML (1999). The immunological synapse: a molecular machine controlling T cell activation. Science 285, 221–227. [PubMed: 10398592]

Gwack Y, Feske S, Srikanth S, Hogan PG, and Rao A (2007). Signalling to transcription: store-operated Ca^{2+} entry and NFAT activation in lymphocytes. Cell Calcium 42, 145–156. [PubMed: 17572487]

Hogan PG, Chen L, Nardone J, and Rao A (2003). Transcriptional regulation by calcium, calcineurin, and NFAT. Genes Dev. 17, 2205–2232. [PubMed: 12975316]

Ishihara S, and Schwartz RH (2011). Two-step binding of transcription factors causes sequential chromatin structural changes at the activated IL-2 promoter. J. Immunol 187, 3292–3299. [PubMed: 21832163]

Janelsins BM, Mathers AR, Tkacheva OA, Erdos G, Shufesky WJ, Morelli AE, and Larregina AT (2009). Proinflammatory tachykinins that signal through the neurokinin 1 receptor promote survival of dendritic cells and potent cellular immunity. Blood 113, 3017–3026. [PubMed: 18987361]

Janelsins BM, Sumpter TL, Tkacheva OA, Rojas-Canales DM, Erdos G, Mathers AR, Shufesky WJ, Storkus WJ, Falo LD Jr., Morelli AE, and Larregina AT (2013). Neurokinin-1 receptor agonists bias therapeutic dendritic cells to induce type 1 immunity by licensing host dendritic cells to produce IL-12. Blood 121, 2923–2933. [PubMed: 23365459]

Kawakami T, and Xiao W (2013). Phospholipase C-β in immune cells. Adv. Biol. Regul 53, 249–257. [PubMed: 23981313]

Kiani A, García-Cózar FJ, Habermann I, Laforsch S, Aebischer T, Ehninger G, and Rao A (2001). Regulation of interferon-gamma gene expression by nuclear factor of activated T cells. Blood 98, 1480–1488. [PubMed: 11520798]

Kim KD, Srikanth S, Yee MK, Mock DC, Lawson GW, and Gwack Y (2011). ORAI1 deficiency impairs activated T cell death and enhances T cell survival. J. Immunol 187, 3620–3630. [PubMed: 21873530]

Kim KD, Srikanth S, Tan YV, Yee MK, Jew M, Damoiseaux R, Jung ME, Shimizu S, An DS, Ribalet B, et al. (2014). Calcium signaling via Orai1 is essential for induction of the nuclear orphan receptor pathway to drive Th17 differentiation. J. Immunol 192, 110–122. [PubMed: 24307733]

Kovac JR, Chrones T, Preiksaitis HG, and Sims SM (2006). Tachykinin receptor expression and function in human esophageal smooth muscle. J. Pharmacol. Exp. Ther 318, 513–520. [PubMed: 16714401]

Kremer KN, Kumar A, and Hedin KE (2011). G alpha i2 and ZAP-70 mediate RasGRP1 membrane localization and activation of SDF-1-induced T cell functions. J. Immunol 187, 3177–3185. [PubMed: 21856938]

Kumar A, Humphreys TD, Kremer KN, Bramati PS, Bradfield L, Edgar CE, and Hedin KE (2006). CXCR4 physically associates with the T cell receptor to signal in T cells. Immunity 25, 213–224. [PubMed: 16919488]

Kwatra MM, Schwinn DA, Schreurs J, Blank JL, Kim CM, Benovic JL, Krause JE, Caron MG, and Lefkowitz RJ (1993). The substance P receptor, which couples to Gq/11, is a substrate of beta-adrenergic receptor kinase 1 and 2. J. Biol. Chem 268, 9161–9164. [PubMed: 7683643]

Lai JP, Douglas SD, and Ho WZ (1998). Human lymphocytes express substance P and its receptor. J. Neuroimmunol 86, 80–86. [PubMed: 9655475]

Lai JP, Ho WZ, Kilpatrick LE, Wang X, Tuluc F, Korchak HM, and Douglas SD (2006). Full-length and truncated neurokinin-1 receptor expression and function during monocyte/macrophage differentiation. Proc. Natl. Acad. Sci. USA 103, 7771–7776. [PubMed: 16675550]

Lai JP, Lai S, Tuluc F, Tansky MF, Kilpatrick LE, Leeman SE, and Douglas SD (2008). Differences in the length of the carboxyl terminus mediate functional properties of neurokinin-1 receptor. Proc. Natl. Acad. Sci. USA 105, 12605–12610. [PubMed: 18713853]

Lambrecht BN, Germonpré PR, Everaert EG, Carro-Muino I, De Veer-man M, de Felipe C, Hunt SP, Thielemans K, Joos GF, and Pauwels RA (1999). Endogenously produced substance P contributes to lymphocyte proliferation induced by dendritic cells and direct TCR ligation. Eur. J. Immunol 29, 3815–3825. [PubMed: 10601989]

Liang G, Barker T, Xie Z, Charles N, Rivera J, and Druey KM (2012). Naive T cells sense the cysteine protease allergen papain through protease-activated receptor 2 and propel TH2 immunity. J. Allergy Clin. Immunol 129, 1377–1386.e1313. [PubMed: 22460072]

Manicassamy S, Gupta S, Huang Z, Molkentin JD, Shang W, and Sun Z (2008). Requirement of calcineurin *a* beta for the survival of naive T cells. J. Immunol 180, 106–112. [PubMed: 18097009]

Mathers AR, Tckacheva OA, Janelsins BM, Shufesky WJ, Morelli AE, and Larregina AT (2007). In vivo signaling through the neurokinin 1 receptor favors transgene expression by Langerhans cells and promotes the generation of Th1- and Tc1-biased immune responses. J. Immunol 178, 7006–7017. [PubMed: 17513750]

McNeil BD, Pundir P, Meeker S, Han L, Undem BJ, Kulka M, and Dong X (2015). Identification of a mast-cell-specific receptor crucial for pseudo-allergic drug reactions. Nature 519, 237–241. [PubMed: 25517090]

Milligan G, Ward RJ, and Marsango S (2019). GPCR homo-oligomerization. Curr. Opin. Cell Biol 57, 40–47. [PubMed: 30453145]

Miyano K, Morioka N, Sugimoto T, Shiraishi S, Uezono Y, and Nakata Y (2010). Activation of the neurokinin-1 receptor in rat spinal astrocytes induces Ca^{2+} release from IP_3-sensitive Ca^{2+} stores and extracellular Ca^{2+} influx through TRPC3. Neurochem. Int 57, 923–934. [PubMed: 20933035]

Mizuta K, Gallos G, Zhu D, Mizuta F, Goubaeva F, Xu D, Panettieri RA Jr., Yang J, and Emala CW Sr.. (2008). Expression and coupling of neurokinin receptor subtypes to inositol phosphate and calcium signaling pathways in human airway smooth muscle cells. Am. J. Physiol. Lung Cell. Mol. Physiol 294, L523–L534. [PubMed: 18203813]

Molon B, Gri G, Bettella M, Gómez-Moutón C, Lanzavecchia A, Martínez-A C, Mañes S, and Viola A (2005). T cell costimulation by chemokine receptors. Nat. Immunol 6, 465–471. [PubMed: 15821738]

Mou L, Xing Y, Kong Z, Zhou Y, Chen Z, and Wang R (2011). The N-terminal domain of human hemokinin-1 influences functional selectivity property for tachykinin receptor neurokinin-1. Biochem. Pharmacol 81, 661–668. [PubMed: 21168392]

Müller MR, Sasaki Y, Stevanovic I, Lamperti ED, Ghosh S, Sharma S, Gelinas C, Rossi DJ, Pipkin ME, Rajewsky K, et al. (2009). Requirement for balanced Ca/NFAT signaling in hematopoietic and embryonic development. Proc. Natl. Acad. Sci. USA 106, 7034–7039. [PubMed: 19351896]

Nederpelt I, Bleeker D, Tuijt B, IJzerman AP, and Heitman LH (2016). Kinetic binding and activation profiles of endogenous tachykinins targeting the NK1 receptor. Biochem. Pharmacol 118, 88–95. [PubMed: 27501920]

Nessler S, Stadelmann C, Bittner A, Schlegel K, Gronen F, Brueck W, Hemmer B, and Sommer N (2006). Suppression of autoimmune encephalomyelitis by a neurokinin-1 receptor antagonist—a putative role for substance P in CNS inflammation. J. Neuroimmunol 179, 1–8. [PubMed: 16904192]

Ngai J, Inngjerdingen M, Berge T, and Taskén K (2009). Interplay between the heterotrimeric G-protein subunits Galphaq and Galphai2 sets the threshold for chemotaxis and TCR activation. BMC Immunol. 10, 27. [PubMed: 19426503]

Niizeki H, Kurimoto I, and Streilein JW (1999). A substance P agonist acts as an adjuvant to promote hapten-specific skin immunity. J. Invest. Dermatol 112, 437–442. [PubMed: 10201526]

Nohara LL, Stanwood SR, Omilusik KD, and Jefferies WA (2015). Tweeters, woofers and horns: the complex orchestration of calcium currents in T lymphocytes. Front. Immunol 6, 234. [PubMed: 26052328]

Oh-Hora M, Yamashita M, Hogan PG, Sharma S, Lamperti E, Chung W, Prakriya M, Feske S, and Rao A (2008). Dual functions for the endoplasmic reticulum calcium sensors STIM1 and STIM2 in T cell activation and tolerance. Nat. Immunol 9, 432–443. [PubMed: 18327260]

Peng SL, Gerth AJ, Ranger AM, and Glimcher LH (2001). NFATc1 and NFATc2 together control both T and B cell activation and differentiation. Immunity 14, 13–20. [PubMed: 11163226]

Popov A, Mirkov I, Miljković D, Belij S, Zolotarevski L, Kataranovski D, and Kataranovski M (2011). Contact allergic response to dinitrochlorobenzene (DNCB) in rats: insight from sensitization phase. Immunobiology 216, 763–770. [PubMed: 21281978]

Porter CM, and Clipstone NA (2002). Sustained NFAT signaling promotes a Th1-like pattern of gene expression in primary murine CD^{4+} T cells. J. Immunol 168, 4936–4945. [PubMed: 11994444]

Quartara L, and Maggi CA (1997). The tachykinin NK1 receptor. Part I: Ligands and mechanisms of cellular activation. Neuropeptides 31, 537–563. [PubMed: 9574822]

Quartara L, and Maggi CA (1998). The tachykinin NK1 receptor. Part II: Distribution and pathophysiological roles. Neuropeptides 32, 1–49. [PubMed: 9571643]

Quinlan KL, Naik SM, Cannon G, Armstrong CA, Bunnett NW, Ansel JC, and Caughman SW (1999). Substance P activates coincident NF-AT-and NF-kappa B-dependent adhesion molecule gene expression in microvascular endothelial cells through intracellular calcium mobilization. J. Immunol 163, 5656–5665. [PubMed: 10553096]

Reinke EK, Johnson MJ, Ling C, Karman J, Lee J, Weinstock JV, Sandor M, and Fabry Z (2006). Substance P receptor mediated maintenance of chronic inflammation in EAE. J. Neuroimmunol 180, 117–125. [PubMed: 16942803]

Rycroft BK, Vikman KS, and Christie MJ (2007). Inflammation reduces the contribution of N-type calcium channels to primary afferent synaptic transmission onto NK1 receptor-positive lamina I neurons in the rat dorsal horn. J. Physiol 580, 883–894. [PubMed: 17303639]

Sánchez-Fernández G, Cabezudo S, García-Hoz C, Benincá C, Aragay AM, Mayor F Jr., and Ribas C (2014). Gαq signalling: the new and the old. Cell. Signal 26, 833–848. [PubMed: 24440667]

Santoni G, Perfumi MC, Spreghini E, Romagnoli S, and Piccoli M (1999). Neurokinin type-1 receptor antagonist inhibits enhancement of T cell functions by substance P in normal and neuromanipulated capsaicin-treated rats. J. Neuroimmunol 93, 15–25. [PubMed: 10378865]

Santoni G, Amantini C, Lucciarini R, Pompei P, Perfumi M, Nabissi M, Morrone S, and Piccoli M (2002). Expression of substance P and its neurokinin-1 receptor on thymocytes: functional relevance in the regulation of thymocyte apoptosis and proliferation. Neuroimmunomodulation 10, 232–246. [PubMed: 12584411]

Sekiya T, and Yoshimura A (2016). In vitro Th differentiation protocol. Methods Mol. Biol 1344, 183–191. [PubMed: 26520124]

Seybold VS, Coicou LG, Groth RD, and Mermelstein PG (2006). Substance P initiates NFAT-dependent gene expression in spinal neurons. J. Neurochem 97, 397–407. [PubMed: 16539671]

Siebenhaar F, Sharov AA, Peters EM, Sharova TY, Syska W, Mardaryev AN, Freyschmidt-Paul P, Sundberg JP, Maurer M, and Botchkarev VA (2007). Substance P as an immunomodulatory neuropeptide in a mouse model for autoimmune hair loss (*Alopecia areata*). J. Invest. Dermatol 127, 1489–1497. [PubMed: 17273166]

Spitsin S, Pappa V, and Douglas SD (2018). Truncation of neurokinin-1 receptor-Negative regulation of substance P signaling. J. Leukoc. Biol 103, 1043–1051, Published online January 10, 2018. 10.1002/JLB.3MIR0817-348R.

Stanners J, Kabouridis PS, McGuire KL, and Tsoukas CD (1995). Interaction between G proteins and tyrosine kinases upon T cell receptor.CD3-mediated signaling. J. Biol. Chem 270, 30635–30642. [PubMed: 8530500]

Steinhoff MS, von Mentzer B, Geppetti P, Pothoulakis C, and Bunnett NW (2014). Tachykinins and their receptors: contributions to physiological control and the mechanisms of disease. Physiol. Rev 94, 265–301. [PubMed: 24382888]

Strainic MG, Liu J, Huang D, An F, Lalli PN, Muqim N, Shapiro VS, Dubyak GR, Heeger PS, and Medof ME (2008). Locally produced complement fragments C5a and C3a provide both costimulatory and survival signals to naive CD4+ T cells. Immunity 28, 425–435. [PubMed: 18328742]

Sumpter TL, Ho CH, Pleet AR, Tkacheva OA, Shufesky WJ, Rojas-Canales DM, Morelli AE, and Larregina AT (2015). Autocrine hemokinin-1 functions as an endogenous adjuvant for IgE-mediated mast cell inflammatory responses. J. Allergy Clin. Immunol 135, 1019–1030.e1018. [PubMed: 25201259]

Sundrud MS, and Rao A (2007). New twists of T cell fate: control of T cell activation and tolerance by TGF-beta and NFAT. Curr. Opin. Immunol 19, 287–293. [PubMed: 17433870]

Taracanova A, Alevizos M, Karagkouni A, Weng Z, Norwitz E, Conti P, Leeman SE, and Theoharides TC (2017). SP and IL-33 together markedly enhance TNF synthesis and secretion from human mast cells mediated by the interaction of their receptors. Proc. Natl. Acad. Sci. USA 114, E4002–E4009. [PubMed: 28461492]

Tuluc F, Lai JP, Kilpatrick LE, Evans DL, and Douglas SD (2009). Neurokinin 1 receptor isoforms and the control of innate immunity. Trends Immunol. 30, 271–276. [PubMed: 19427266]

Vilisaar J, Kawabe K, Braitch M, Aram J, Furtun Y, Fahey AJ, Chopra M, Tanasescu R, Tighe PJ, Gran B, et al. (2015). Reciprocal regulation of substance P and IL-12/IL-23 and the associated cytokines, IFNg/IL-17: a perspective on the relevance of this interaction to multiple sclerosis. J. Neuroimmune Pharmacol 10, 457–467. [PubMed: 25690155]

Weinstock JV (2004). The role of substance P, hemokinin and their receptor in governing mucosal inflammation and granulomatous responses. Front. Biosci 9, 1936–1943. [PubMed: 14977599]

Weinstock JV (2015). Substance P and the regulation of inflammation in infections and inflammatory bowel disease. Acta Physiol. (Oxf.) 213, 453–461. [PubMed: 25424746]

Williams R, Zou X, and Hoyle GW (2007). Tachykinin-1 receptor stimulates proinflammatory gene expression in lung epithelial cells through activation of NF-kappaB via a G(q)-dependent pathway. Am. J. Physiol. Lung Cell. Mol. Physiol 292, L430–L437. [PubMed: 17041011]

Zambricki E, Shigeoka A, Kishimoto H, Sprent J, Burakoff S, Carpenter C, Milford E, and McKay D (2005). Signaling T-cell survival and death by IL-2 and IL-15. Am. J. Transplant 5, 2623–2631. [PubMed: 16212621]

Zhang H, Cang CL, Kawasaki Y, Liang LL, Zhang YQ, Ji RR, and Zhao ZQ (2007). Neurokinin-1 receptor enhances TRPV1 activity in primary sensory neurons via PKCepsilon: a novel pathway for heat hyperalgesia. J. Neurosci 27, 12067–12077. [PubMed: 17978048]

Zhang L, and Shi G (2016). Gq-coupled receptors in autoimmunity. J. Immunol. Res 2016, 3969023. [PubMed: 26885533]

Zhang Y, Lu L, Furlonger C, Wu GE, and Paige CJ (2000). Hemokinin is a hematopoietic-specific tachykinin that regulates B lymphopoiesis. Nat. Immunol 1, 392–397. [PubMed: 11062498]

Zhang Y, and Paige CJ (2003). T-cell developmental blockage by tachykinin antagonists and the role of hemokinin 1 in T lymphopoiesis. Blood 102, 2165–2172. [PubMed: 12791665]

Highlights

- T cells express the neurokinin 1 receptor (NK1R) and synthesize its agonists
- The NK1R and its agonists co-localize in or near the T cell: APC immune synapse
- The NK1R promotes optimal Ca^{2+} flux and survival of TCR-activated T cells
- Lack of the NK1R or its agonists results in deficient Th1-/Th17-biased immunity

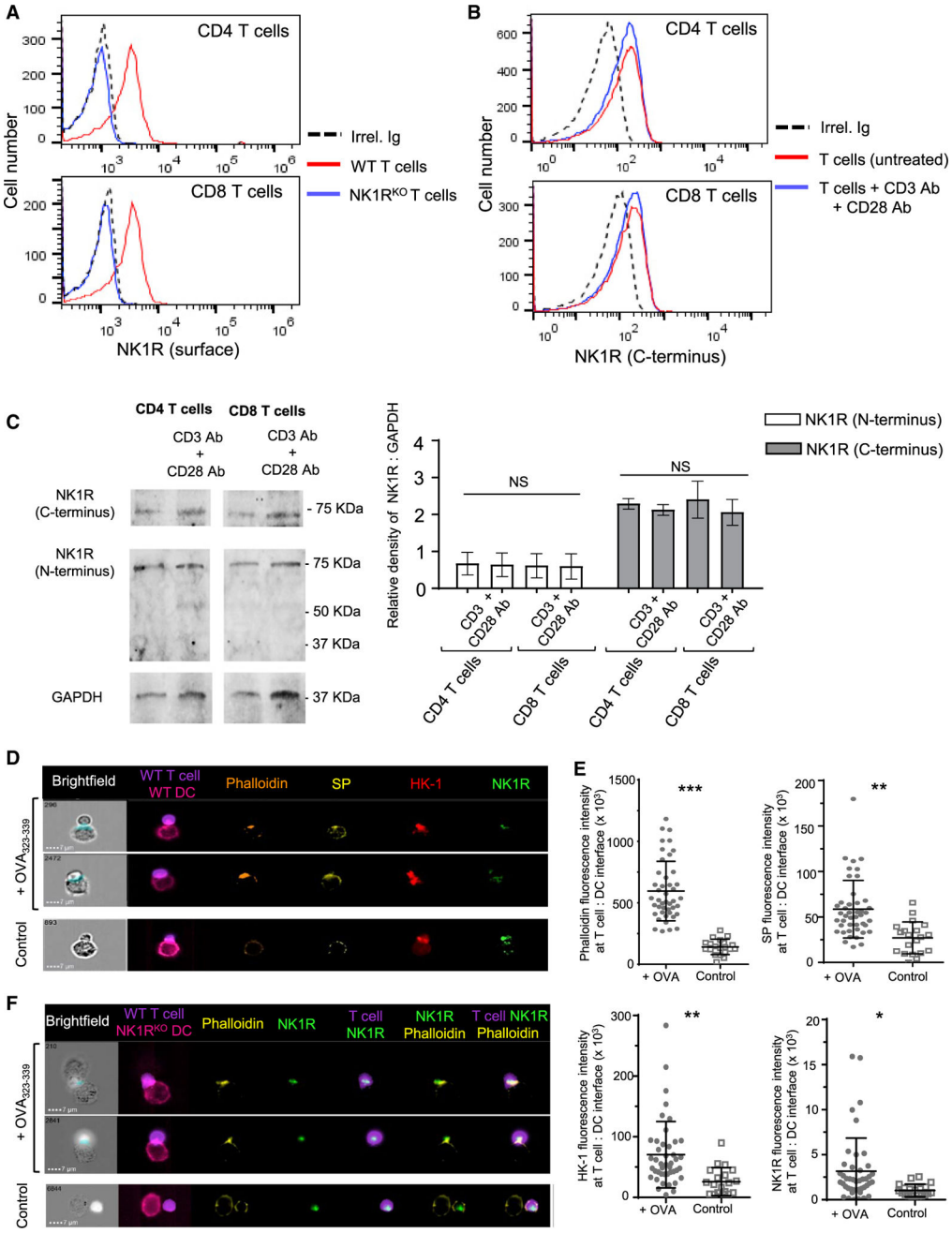

Figure 1. T Cells Express the f-NK1R that Is Recruited at the Immune Synapse

(A) NK1R (extracellular) expression by FACS on WT T cells and control NK1R^{KO} T cells.

(B) FACS analysis of NK1R (C terminus) on permeabilized WT T cells, untreated or after 24-h activation with CD3 and CD28 Ab.

(C) Western blot of NK1R in T cells untreated or after 24 h incubation with CD3 and CD28 Ab. The 75-kDa band corresponds to glycosylated f-NK1R. One representative experiment of 3. Bar diagram: relative density of f-NK1R normalized to GAPDH. Results pooled from two experiments. Means ± 1 SD.

(D) ImageStream of doublets of OT-II CD4 T cells and B6 DC loaded with OVA323–339 or not (Control). SP, HK-1, and the NK1R concentrate at the T cell-DC synapse (light blue mask), identified by rearrangement of F-actin labeled with Texas red-phalloidin.
(E) Comparison by ImageStream of relative fluorescence intensities of phalloidin, SP, HK-1, and NK1R within the interface mask on doublets of OT-II T cells and B6 DC loaded with $OVA_{323–339}$ (+ OVA) or not (Control).
(F) ImageStream of doublets of OT-II T cells and B6 $NK1R^{KO}$ DC loaded or not (Control) with $OVA_{323–339}$. The NK1R expressed by OT-II cells concentrates at the T cell-DC synapse (light blue mask).
In (A) and (B), one representative experiment of 3. In (D)–(F), 1 of 2 experiments with 5,000 cells collected in each. Data were analyzed by 1-way ANOVA followed by *ad hoc* Student Newman Keuls test (C) and 2-tailed Student's t test (E). *$p < 0.05$, **$p < 0.01$, ***$p < 0.001$, NS, not significant.

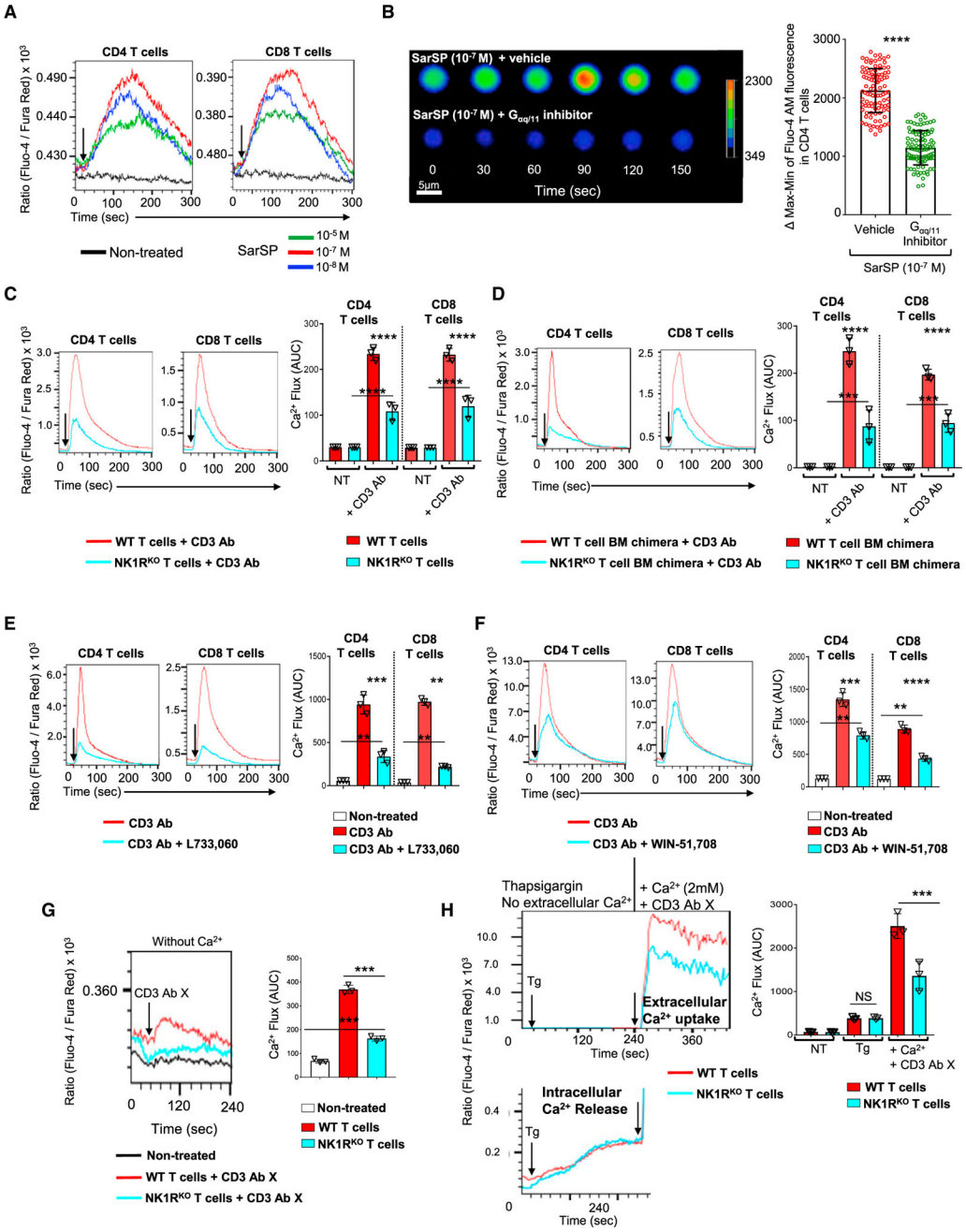

Figure 2. NK1R-signaling Per Se Promotes Ca^{2+} Flux in T Cells and Potentiates the Ca^{2+} Flux Triggered by the T Cell Receptor (TCR)

(A) Ca^{2+} flux by ratiometric assay by FACS in T cells exposed to SarSP added after acquisition of the 30-s baseline (arrows).

(B) Live-cell imaging of Ca^{2+} flux in T cells exposed to SarSP alone or with the $G_{\alpha q/11}$ inhibitor YM-254,890. Ca^{2+} flux was analyzed during 10 min after adding SarSP and images were acquired every 30 s. Representative cells out of 200. Heat bar: Fluo-4-AM fluorescence intensity from blue (minimum) to red (maximum) that correlates directly with Ca^{2+} flux. Bar diagram: quantification of Fluo-4-AM signal on 200 individual cells,

recorded for 10 min. Ca^{2+} flux on each cell was calculated by the difference between the maximal and minimal intensity of Fluo-4-AM fluorescence (peak value).

(C and D) Ratiometric assays of Ca^{2+} flux by FACS in T cells from WT or global $NK1R^{KO}$ mice (C), or from WT or $NK1R^{KO}$ BM T cell chimeras (D) untreated of stimulated by CD3 Ab cross linking (arrows). Bar diagrams: area under the curve (AUC) of Ca^{2+} flux. Each symbol corresponds to T cells from a different mouse analyzed in the same experiment.

(E and F) Ratiometric assays of Ca^{2+} flux by FACS in T cells untreated or exposed to the NK1R antagonists L733,060 (E) or WIN-51,708 (F) and stimulated by CD3 Ab cross linking (arrows). Bar diagrams: AUC of Ca^{2+} flux. Each dot corresponds to T cells from a different mouse.

(G) Ratiometric assay by FACS of intracellular Ca^{2+} efflux in WT and $NK1R^{KO}$ T cells following stimulation by CD3 Ab cross linking (X, arrow) in Ca^{2+}-free media.

(H) Ratiometric assay of Ca^{2+} influx by FACS in WT and $NK1R^{KO}$ T cells treated with thapsigargin (solid arrows) in Ca^{2+}-free media for 4 min and then stimulated by CD3 Ab cross linking (X, dash arrows) in the presence of Ca^{2+}.

(G and H) One representative experiment out of 2. In (A) and (C)–(H), baselines were recorded for 30 s before addition of stimuli. Results were analyzed by 1-way ANOVA followed by *ad hoc* Student Newman Keuls test (C–H) and 2-tailed Student's t test (B). **p < 0.01, ***p < 0.001, ****p < 0.0001, NS, not significant.

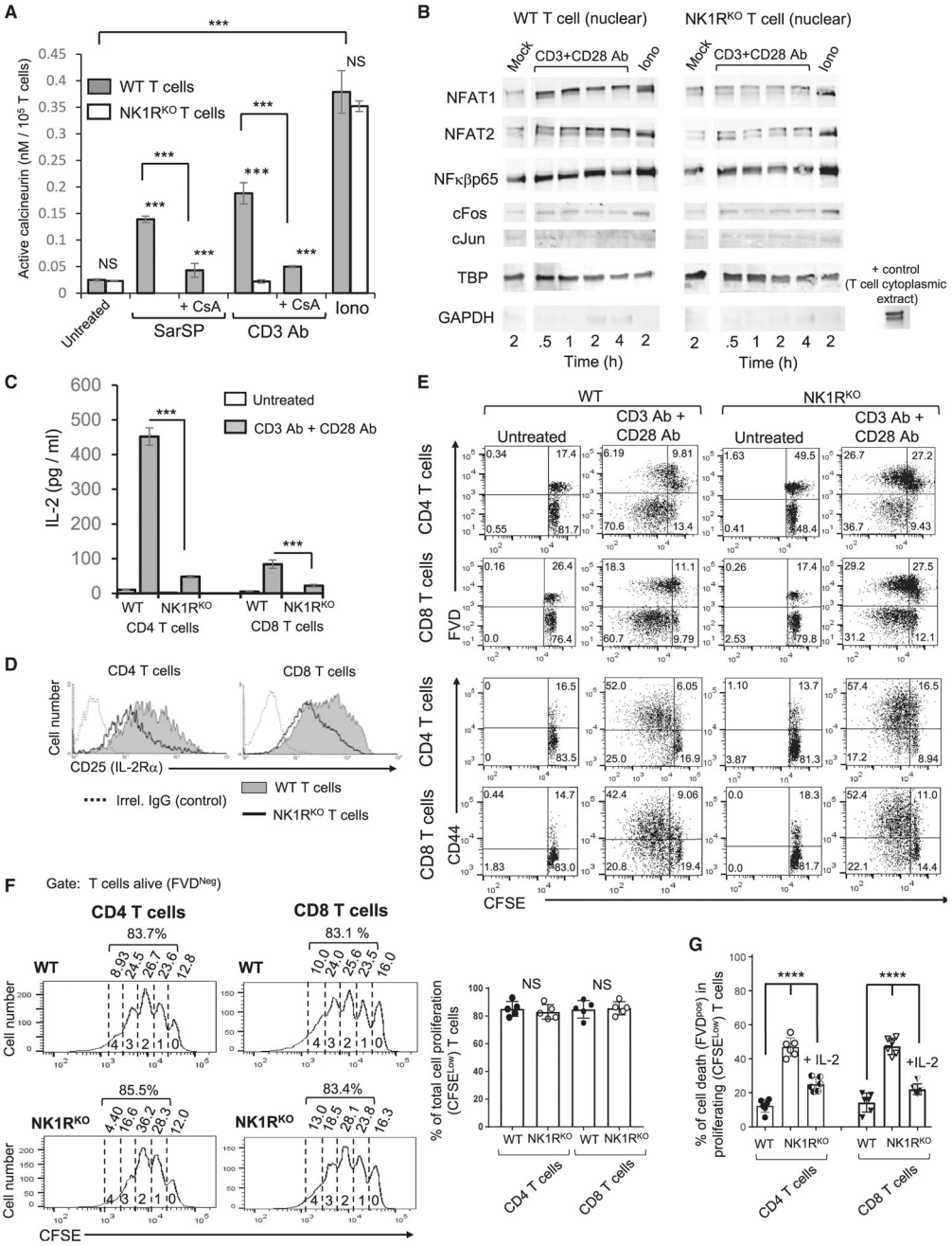

Figure 3. NK1R-signaling Promotes Activation of NFAT1, NFAT2, and NFκb-p65, and T Cell Survival Dependent on IL-2 Secretion

(A) Calcineurin activity in WT and NK1R^{KO} T cells incubated with SarSP or CD3 Ab, measured 15 min after treatment. Means ± 1 SD of duplicated results of 1 representative experiment of 2.

(B) Western blot analysis of NFAT1, NFAT2, NFκβ-p65, cFos, and cJun, in nuclear extracts of WT and NK1R^{KO} T cells, untreated or after incubation with CD3 and CD28 Ab. Controls were stimulated with ionomycin (Iono). One representative experiment of 3.

(C) Concentrations of IL-2 by ELISA in supernatants of WT and NK1R^{KO} T cells untreated or after 24-h stimulation with CD3 and CD28 Ab. Means ± 1 SD, 1 representative of 3 experiments.
(D) Surface IL-2Rα expression by FACS in WT and NK1R^{KO} T cells untreated or after 24-h stimulation with CD3 and CD28 Ab. One representative of 3 experiments.
(E) Comparison by FACS of T cell proliferation (CFSE dilution), cell death (FVD incorporation), and activation (CD44^{High}) between WT and NK1R^{KO} T cells after 4-day stimulation with CD3 and CD28 Ab. Numbers are cell percentages per quadrant. One representative out of 6 experiments.
(F) Comparison by FACS of cycles of cell division (histograms) and percentages of cell proliferation (bar diagram) between WT and NK1R^{KO} T cells. Numbers in histograms are cell percentages. Each dot in the bar diagrams represents a mouse. Means ± 1 SD.
(G) Percentages of cell death (by FVD incorporation) of WT and NK1R^{KO} T cells stimulated for 4 days with CD3 and CD28 Ab, alone or plus IL-2. Means ± 1 SD, 6 mice per condition.
Results were analyzed by 1-way ANOVA followed by *ad hoc* Student Newman Keuls test (A, C, F, and G). ***p < 0.001, ****p < 0.0001, NS: not significant.

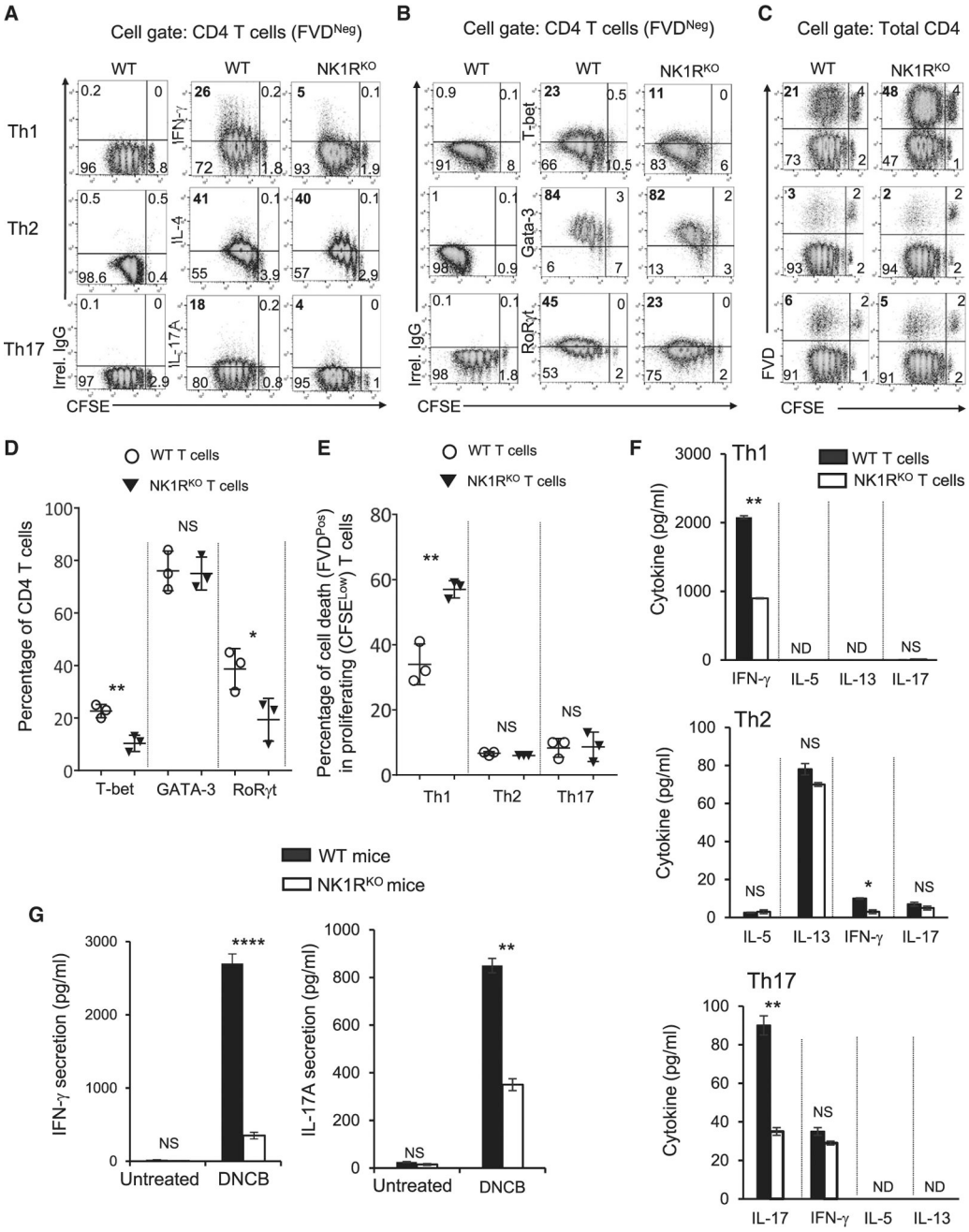

Figure 4. Effect of NK1R-signaling on Polarization of CD4 T Cells

(A) FACS analysis of proliferation (CFSE dilution) and intracellular cytokines in Th1 (IFN-γ)-, Th2 (IL-4)-, and Th17 (IL-17A)-polarized WT and NK1R^{KO} CD4 T cells.

(B) Comparison by FACS of expression of Th1 (T-bet), Th2 (GATA-3), and Th17 (RoRγt) transcription factors between WT and NK1R^{KO} CD4 T cells cultured under polarizing conditions.

(C) Assessment by FACS of cell death (by FVD incorporation) in WT and NK1R^{KO} CD4 T cells polarized *in vitro* into Th1, Th2, or Th17 cells. In (A)–(C), numbers are cell percentages per quadrant. One representative experiment out of 3.

(D) Quantification of WT and NK1R^{KO} CD4 T cells expressing T-bet (Th1), GATA-3 (Th2), or RoRγt (Th17) after culture under polarizing conditions, analyzed by FACS. Each dot represents an independent experiment. Means ± 1 SD.

(E) Quantification of cell death (by FVD incorporation) in proliferating (CFSE^{Low}) WT and NK1R^{KO} CD4 T cells from (C). Each dot represents an individual experiment. Means ± 1 SD.

(F) Concentrations of cytokines in supernatants of WT and NK1R^{KO} CD4 T cells cultured for 4 days under polarizing conditions. Duplicates from 1 experiment representative of 3. Means ± 1 SD.

(G) Secretion of IFN-γ and IL-17 by T cells homing in draining lymph nodes of skin sensitized with DNCB 5 days prior. Means ± 1 SD of 4 mice per variable. Data were analyzed by 1-way ANOVA followed by *ad hoc* Student Newman Keuls test (D–G). *$p < 0.05$, **$p < 0.01$, ****$p < 0.0001$, NS, not significant.

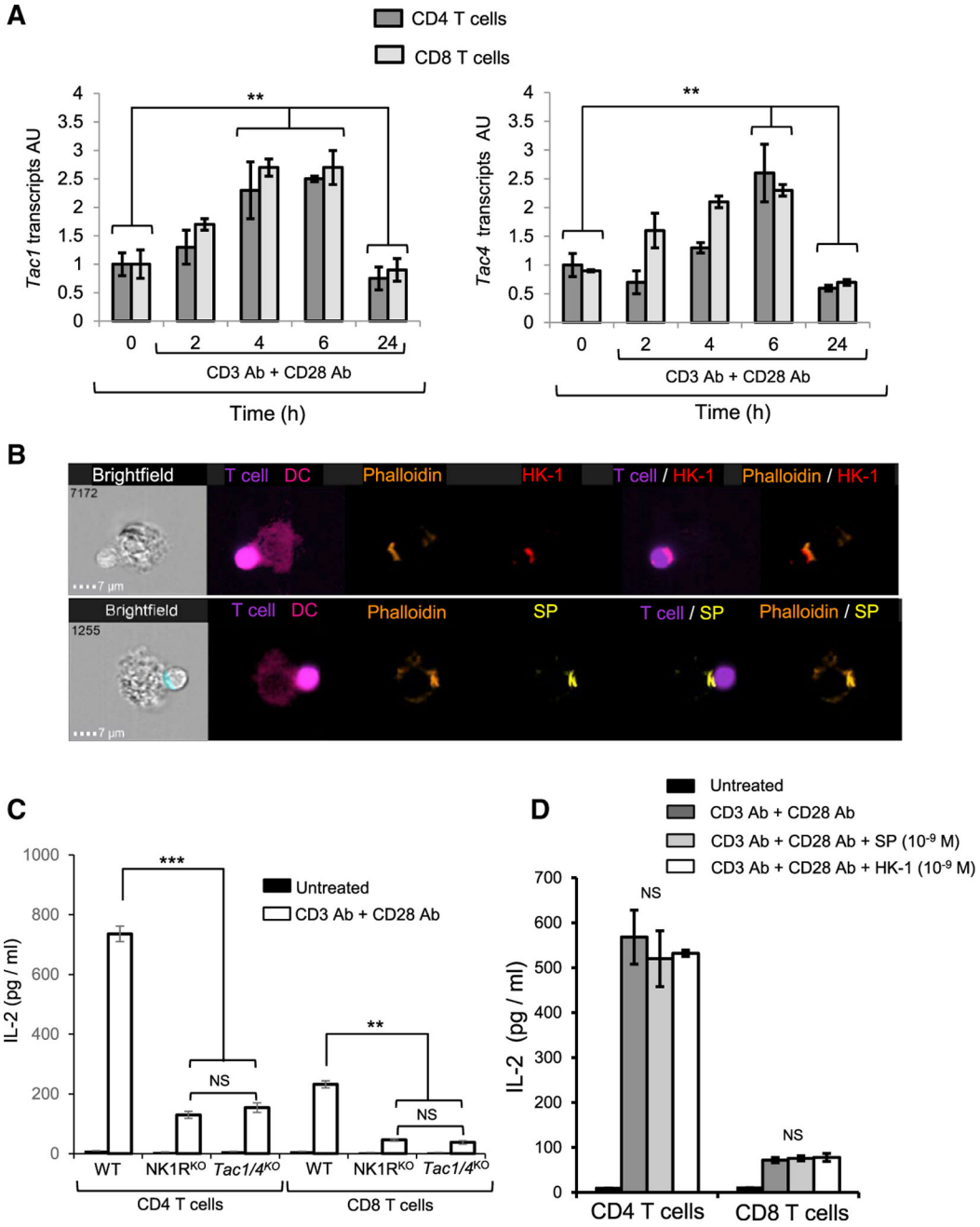

Figure 5. Autocrine SP and HK-1 Promote IL-2 Secretion and Survival of T Cells

(A) Quantification of *Tac1* and *Tac4* transcripts by RT-qPCR in CD4 or CD8 T cells before and following stimulation with CD3 and CD28 Ab during 2, 4, 6, and 24 h. Means ± 1 SD of 2 independent experiments.

(B) ImageStream of cell doublets composed of OT-II CD4 T cells and *Tac1/4*$^{\text{Double KO}}$ B6 BMDC loaded with $OVA_{323–339}$. SP and HK-1 concentrate within the area of the T cell-DC synapse (light blue mask) identified by rearrangement of F-actin visualized by staining with Texas red-phalloidin.

(C) Concentration of IL-2 (by ELISA) in 24-h supernatants of WT, $NK1R^{KO}$, and *Tac1*/*4*$^{\text{Double KO}}$ T cells cultured untreated or with CD3 and CD28 Ab. Means ± 1 SD of 3 experiments.

(D) Concentrations of IL-2 (by ELISA) in supernatants of T cells cultured untreated, with CD3 and CD28 Ab alone or plus exogenous SP or HK-1. Means ± 1 SD of 3 experiments. Results were analyzed by 1-way ANOVA followed by *ad hoc* Student Newman Keuls test (A, C, and D). **p < 0.01, ***p < 0.001, NS: not significant.

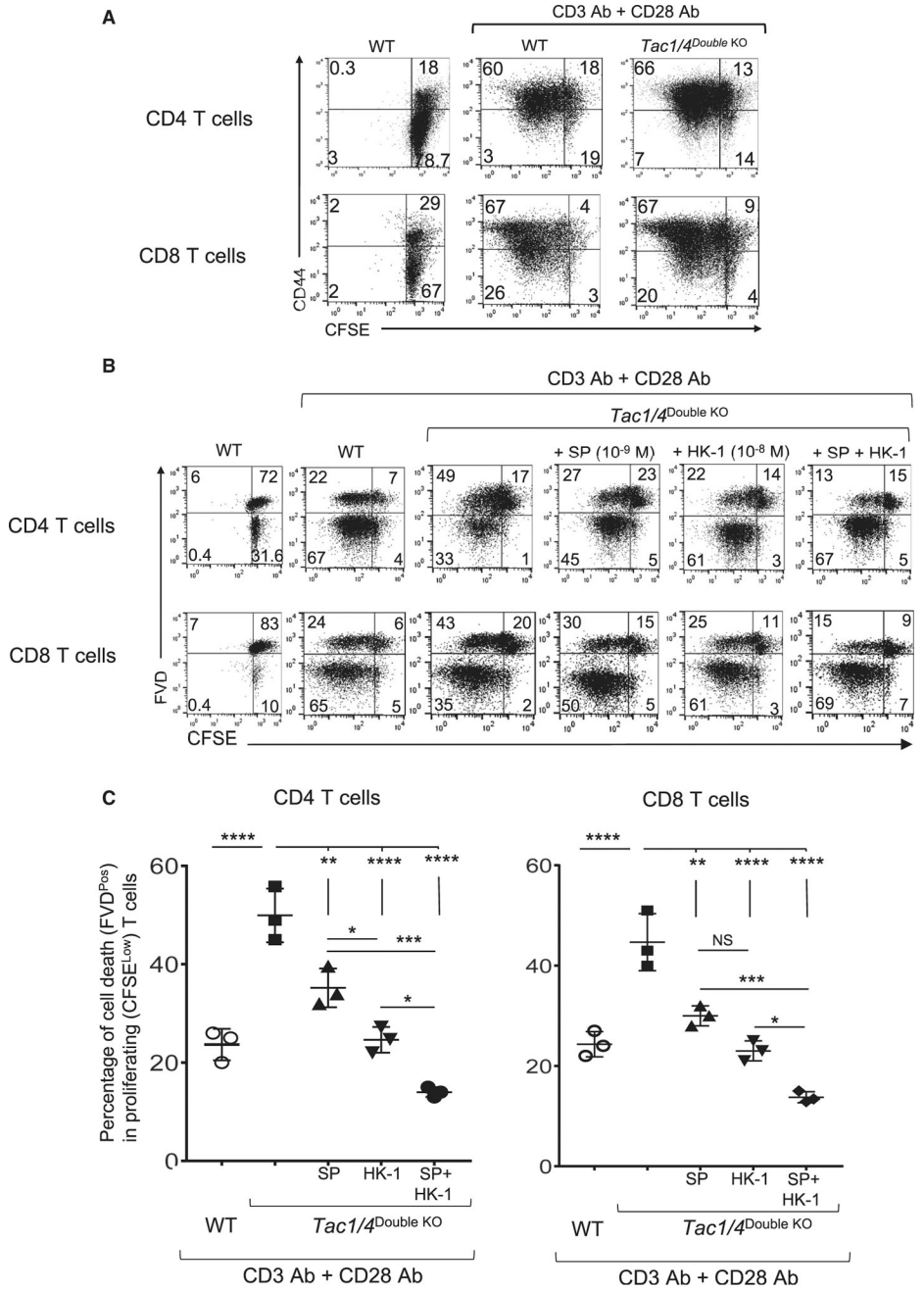

Figure 6. NK1R-Signaling by Autocrine SP and HK-1 Promotes T Cell Survival

(A) FACS analysis of proliferation (CFSE dilution) and activation ($CD44^{high}$) of WT or *Tac1/4*$^{Double\ KO}$ T cells, the latter unable to synthetize SP and HK-1, kept in culture for 4 days untreated or with CD3 and CD28 Ab. Numbers are cell percentages per quadrant. One representative experiment of 5.

(B) Proliferation (CFSE dilution) and cell death (FVD incorporation) analyzed by FACS on WT and *Tac1/4*$^{Double\ KO}$ T cells cultured for 4 days untreated or with CD3 and CD28 Ab alone, or plus exogenous SP, HK-1, or both. Numbers are cell percentages per quadrant. One representative of 3 experiments.

(C) Quantification of cell death (FVD incorporation) in dividing ($CFSE^{Low}$) WT and *Tac1/4*$^{Double\ KO}$ T cells from the experiments shown in (B). Each dot represents an independent experiment. Means ± 1 SD.

Results in (C) were analyzed by 1-way ANOVA followed by *ad hoc* Student Newman Keuls test. *p < 0.05, **p < 0.01, ***p < 0.001, ****p < 0.0001, NS, not significant.

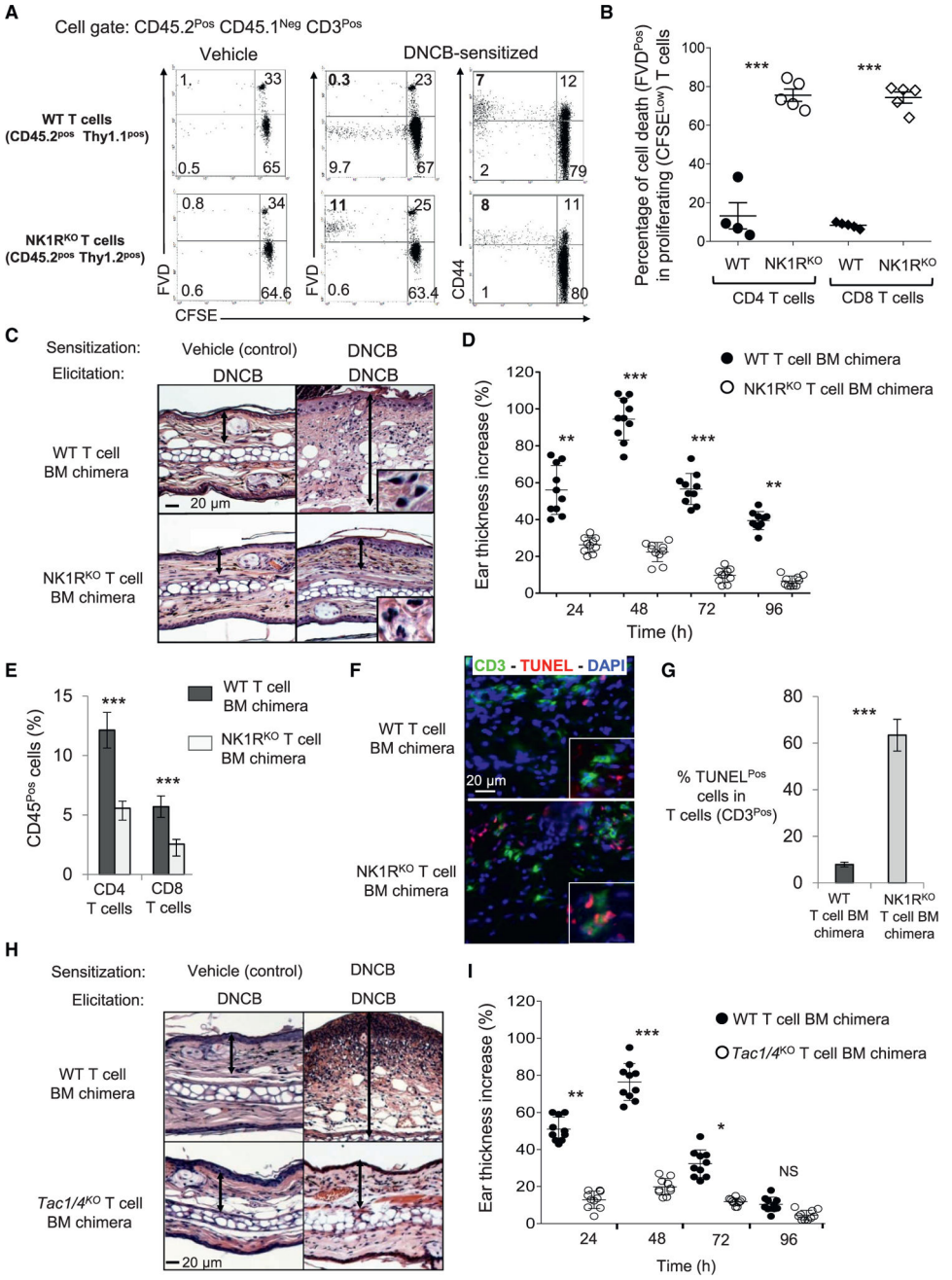

Figure 7. *In Vivo* Signaling of the NK1R Sustains T Cell Survival during Priming and the Effector Phase of Contact Dermatitis

(A) Proliferation (CFSE dilution), activation ($CD44^{High}$), and cell death (FVD incorporation) of CFSE-labeled WT (CD45.2 Thy1.1) and $NK1R^{KO}$ (CD45.2 Thy1.2) T cells i.v. injected in B6 (CD45.1) mice, analyzed by FACS in inguinal lymph nodes draining skin sensitized with DNCB, 5 days prior.

(B) Quantification of cell death (FVD incorporation) in i.v.-transferred CFSE-labeled WT and $NK1R^{KO}$ T cells that proliferated ($CFSE^{Low}$) in response to DNCB sensitization on the abdominal skin. Each dot represents inguinal lymph nodes pooled from an individual mouse. Means ± 1 SD, 4–5 mice per condition. Numbers are cell percentages per quadrant.

(C) Images of tissue sections of the elicitation site (ear) of $NK1R^{KO}$ T cell and WT T cell BM chimeras, 48 h after DTH elicitation. The leukocyte infiltrate and edema (arrows) are more prominent in skin of control WT T cell BM chimeras. Insets: leukocyte infiltrate. H&E, X 200–500.

(D) Percentages of ear thickness increase in $NK1R^{KO}$ T cell and WT T cell BM chimeras after DTH elicitation. Means ± 1 SD, 10 mice per group.

(E) Percentage of T cells in the CD45 gate of cell suspensions from the elicitation site (ear skin) of WT and $NK1R^{KO}$ T cell BM chimeras, analyzed 48 h after DTH elicitation.

(F) Histological analysis of the DTH elicitation site (ear skin) of T cell BM chimeras showing T cells (green) undergoing apoptosis ($TUNEL^{Pos}$, red). Nuclei were stained blue with DAPI. X 200–500.

(G) Bar diagram with percentages of T cells labeled by TUNEL at the DTH elicitation site. Means ± 1 SD, 10 individual samples.

(H) Images of tissue sections of the elicitation site (ear skin) of *Tac1/4*$^{\text{Double KO}}$ T cell BM chimeras and control WT T cell BM chimeras collected 48 h after DTH elicitation. The elicitation site of control chimeras exhibited more prominent leukocyte infiltration and edema (arrows) than the skin of *Tac1/4*$^{\text{Double KO}}$ T cell BM chimeras (H&E, X 200).

(I) Percentages of ear thickness increase in *Tac1/4*$^{\text{Double KO}}$ T cell BM chimeras and control WT T cell BM chimeras, measured after 24, 48, 72, and 96 h following DTH elicitation. Means ± 1 SD of 10 mice per group.

Data were analyzed by 1-way ANOVA followed by *ad hoc* Student Newman Keuls test (B, D, and I) and 2-tailed Student's t test (E and G). *$p < 0.05$, **$p < 0.01$, ***$p < 0.001$, NS, not significant.

KEY RESOURCES TABLE

REAGENT or RESOURCE	SOURCE	IDENTIFIER
Antibodies		
Anti-mouse CD3ε (Clone 145-2C11), functional grade	eBioscience	Cat # 16-0031-82
Anti-mouse CD3ε (Clone 145-2C11), biotin	eBioscience	Cat # 13-0031-85
Anti-mouse CD3ε (Clone 145-2C11), PE-Cy5	eBioscience	Cat # 15-0031-82
Anti-mouse CD3ε (Clone 145-2C11), PE-Cy7	BD	Cat # 552774
Anti-mouse CD3 (Clone 17A2), APC	eBioscience	Cat # 17-0032-82
Anti-mouse CD4 (Clone GK1.5), APC	eBioscience	Cat # 17-0041-82
Anti-mouse CD4 (Clone RM4-5), BUV395	BD	Cat # 740208
Anti-Mouse CD4 (Clone RM4-5), V450	BD	Cat # 560468
Anti-mouse CD8α (Clone 53-6.7), PE-Cy7	BD	Cat # 552877
Anti-mouse CD8α (Clone 53-6.7), Pacific blue	BD	Cat # 558106
Anti-mouse CD8α (Clone 53-6.7), PE-Cy5	BD	Cat # 553034
Anti-mouse CD8α (Clone 53-6.7), V500	BD	Cat # 560776
Anti-mouse CD8α (Clone 53-6.7), APC	BioLegend	Cat # 100712
Anti-mouse CD8β (Clone eBioH35-17.2), FITC	eBioscience	Cat # 11-0083-82
Anti-mouse CD11 b (Clone Ml/70), FITC	eBioscience	Cat # 11-0112-82
Anti-mouse CD11c (Clone HL3), APC-Cy7	BD	Cat # 561241
Anti-mouse CD19 (Clone 1D3)	Invitrogen	Cat # MA1-10128
Anti-mouse CD19 (Clone 1D3), FITC	eBiosciences	Cat # 11-0193-82
Anti-mouse CD25 (Clone PC61.5)	eBioscience	Cat # 16-0251-85
Anti-mouse CD25 (Clone PC61.5), BUV395	BD	Cat # 564022
Anti-mouse CD25 (Clone PC61.5), FITC	eBioscience	Cat # 11-0251-82
Anti-mouse CD28 (Clone 37.51)	BD	Cat # 557393
Anti-mouse CD44 (Clone IM7), PE	Invitrogen / eBioscience	Cat # 12-0441-82
Anti-mouse CD44 (Clone IM7), eFluor450®	eBioscience	Cat # 48-0441-82
Anti-mouse CD45.1 (Clone A20), PE-Cy5	Invitrogen / eBioscience	Cat # 15-0453-82
Anti-mouse CD45.2 (Clone 104), FITC	BioLegend	Cat # 109805
Anti-mouse CD45R / B220 (Clone Ra3-6B2), FITC	BioLegend	Cat # 103205
Anti-mouse CD62L (Clone MEL-14), PE	Invitrogen / eBioscience	Cat # 12-0621-82
Anti-mouse CD62L (Clone MAL-14), PE-Cy5	eBiosciences	Cat # 15-0621-82
Anti-mouse CD90.1 /Thy1.1 (Clone OX-7), BUV395	BD	Cat # 740261
Anti-mouse CD90.2 / Thy1.2 (Clone 53-2.1), PE-Cy7	Invitrogen / eBioscience	Cat # 25-0902-82
Anti-mouse NK1.1 (Clone PK136), FITC	Invitrogen	Cat # 11-5941-82
Anti-mouse IL-2 (Clone JES6-5H4), FITC	BD	Cat # 554427
Anti-mouse IL4 (Clone 11B11), functional grade	BioXcell	Cat # BE0045
Anti-mouse IL4 (Clone 11B11), PE	BD	Cat # 554435
Anti-mouse IL17A (Clone TC 11-18 H10), BUV395	BD	Cat # 559502
Anti-mouse IFN-γ (Clone AN-18), functional grade	Thermo Fisher	Cat # 16-7313-81
Anti-mouse IFN-γ (Clone XMG1.2), PerCP-Cy5.5	BD	Cat # 560660
Anti-mouse T-bet (Clone 04-46), PE	BD	Cat # 561268

REAGENT or RESOURCE	SOURCE	IDENTIFIER
Anti-mouse GATA-3 (Clone L50-820), PE	BD	Cat # 560074
Anti-mouse RoRγt (Clone AFJKS-9), PE	Invitrogen / eBioscience	Cat # 12-6988-82
Anti-mouse FoxP3 (Clone FJK-16 s), PE	Invitrogen / eBioscience	Cat # 12-5773-82
Anti-mouse / human NFAT1 (Clone D43B1)	Cell Signaling	Cat # 5861
Anti-mouse / human NFAT1 (Clone D43B1), AF488	Cell Signaling	Cat # 14324
Anti-mouse / human NFAT2 (Clone D15F1)	Cell Signaling	Cat # 8032
Anti-mouse / rat / human NFAT2 (Clone 7A6), AF488	BioLegend	Cat # 649603
Anti-mouse / human NFκB-p65 (C-20, goat polyolonal)	Santa Cruz	Cat # SC-372-G
Anti-mouse / human cFos (K-25, goat polyclonal)	Santa Cruz	Cat # SC-253-G
Anti-mouse / human cJun (D, goat polyclonal)	Santa Cruz	Cat # SC-44-G
Anti-mouse / rat / human PLCγ1 (Clone D9H10)	Cell Signaling	Cat # 5690
Anti-mouse / human Phospho PLCγ1 (Tyr_{783}) (Clone PLCGTYR783-C4), PE	Invitrogen	Cat # MA5-28030
Anti-mouse / rat / human ZAP70 (Clone E267)	Abeam	Cat # ab32410
Anti-mouse / human Phospho ZAP70/Syk (Tyr_{319}, Tyr_{352}) (Clone n3kobu5), PE	eBioscience	Cat # 12-9006-42
Anti-mouse / rat / human TBP (rabbit polyclonal)	Cell Signaling	Cat # 8515S
Anti-mouse / rat / human GAPDH (Clone 1D4)	Novus Biological	Cat # NB300-221
Anti-mouse / rat / human NK1R N terminus (rabbit polyclonal)	Novus Biological	Cat # NB300-119
Anti-mouse / rat / human NK1R C terminus (Clone D-11)	Santa Cruz	Cat # SC-365091
Anti-mouse / rat / human NK1R C terminus (Clone D-11), PE	Santa Cruz	Cat # SC-365091 PE
Anti-mouse / rat / human NK1R extracellular (rabbit polyclonal), ATTO488	Alomone Labs	Cat # ATR-001-AG
Anti-mouse / rat / human Substance P (rabbit polyclonal), Cy3	Bioss USA	Cat # bs-0064R-Cy3
Anti-mouse / rat HK-1 (rabbit polyclonal)	Peninsula Laboratories	T-4835.0400
Anti-goat IgG, IRDye® 800CW	LI-COR	Cat # 926-32214
Anti-rabbit IgG, IRDye® 680LT	LI-COR	Cat # 926-68023
Anti-mouse IgG, IRDye® 680LT	LI-COR	Cat # 926-68022
Anti-mouse IgM, DyLight 800	Thermo Fisher	Cat # SA5-10156
Anti-Armenian hamster IgG	Jackson ImmunoResearch	Cat # 127-005-160
Mouse lgG1 (Clone MOPC-21), isotype control, AF488	Biolegend	Cat # 400129
Rabbit IgG (Clone DA1E), isotype control, AF488	Cell Signaling	Cat # 2975
Armenian Hamster lgG2κ (Clone B81-3)	BD	Cat # 559277
Chemicals, Peptides, and Recombinant Proteins		
Cell Tracker™ Violet	Thermo Fisher	Cat #C10094
CFDA-SE. Dye (CFSE)	Thermo Fisher	Cat #V12883
Fluo-4AM	Thermo Fisher	Cat # 14201
Fura Red AM Cell Permeant	Invitrogen	Cat # MAS-28030
Thapsigargin	Sigma-Aldrich	Cat # 9033
DAPI	Thermo Fisher	Cat # D1306
Fixable Viability Dye eFluor 780	eBioscience	Cat # 65-0865-14
PE Annexin V apoptosis Detection Kit I	BD	Cat # 559763
Propidium Iodide Staining Solution	BD	Cat # 556463
NucView® 405 Caspase-3 Substrate, 1 mM in PBS	Biotium	Cat # 10407
Necrostatin-1	Sigma-Aldrich	Cat # N9037

REAGENT or RESOURCE	SOURCE	IDENTIFIER
Dulbecco's Phosphate Buffered Saline (PBS)	Sigma-Aldrich	Cat # D8662-500
BD GolgiPlug Protein Transport Inhibitor (containing Brefeldin-A)	BD	Cat # 555029
lonomycin calcium salt	Sigma-Aldrich	Cat # I3909
DNCB	Sigma-Aldrich	Cat # 237329
Saponin	Sigma-Aldrich	Cat # 47036
PIPES Free Acid	Research Products International	Cat # P40140-10.0
Triton X-100	Sigma-Aldrich	Cat # X100
[Sar^9, $Met(O_2)^{11}$]-Substance P	Sigma-Aldrich	Cat # S3672
Substance P	Tocris Bioscience	Cat # 1156
Hemokinin 1 (mouse)	Tocris Bioscience	Cat # 1535
L733,060 hydrochloride (NK1R inhibitor)	Tocris Bioscience	Cat # 1145
WIN-51,708 hydrate (NK1R inhibitor)	Sigma-Aldrich	Cat # W1003
YM-254,890, G_q inhibitor ($G\alpha_{q/11}$ inhibitor)	Focus Biomolecules	Cat # 10-1590-0100
Rhodamine Phalloidin	Thermo Fisher	Cat # R415
Texas Red- X Phalloidin	Thermo Fisher	Cat # T7471
Fluorescein Phalloidin	Thermo Fisher	Cat # F432
$OVA_{323–339}$ peptide	Peptide and Peptoid Synthesis Core (Univ. of Pittsburgh)	N/A
Avidin/Biotin Blocking Kit	Vector	Cat # SP-2001
Vectabond Reagent	Vector	Cat # SP-1800
DyLight™ 488-Conjugated Streptavidin	Jackson ImmunoResearch	Cat # 016-480-084
Halt Protease Inhibition Cocktail	Thermo Scientific	Cat # 1862209
RIPA Buffer	Sigma-Aldrich	Cat # R0278-50ML
4x Laemmli Sample Buffer	BIO-RAD	Cat # 1610747
Immun-Blot® Low Fluorescence PVDF/Filter Paper Sets	BIO-RAD	Cat # 1620260
Any kD Mini-PROTEAN® TGX Precast Protein Gels, 10-well, 50 μl	BIO-RAD	Cat # 4569034S
DTT	Sigma-Aldrich	Cat # DTT-RO
Odyssey Blocking Buffer	LI-COR	Cat # 92740000
TRIzol Reagent	Thermo-Fisher	Cat # AM9738
PMA	Sigma-Aldrich	Cat # P1585
Human IL-2 (recombinant)	R&D Systems	Cat # 202-IL-010
Mouse GM-CSF (recombinant)	PeproTech	Cat # 315-03
Mouse IL-4 (recombinant)	PeproTech	Cat # 214-14
Mouse IL-6 (recombinant)	PeproTech	Cat # 216-16
Mouse IL-12p70 (recombinant)	PeproTech	Cat # 210-12
Mouse IL-23 (recombinant)	R&D Systems	Cat # 1887-ML-010
Mouse TGF-β1 (recombinant)	R&D Systems	Cat # 7666-MB
Critical Commercial Assays		
iScript™ Reverse Transcription Supermix for RT-qPCR	Bio-Rad	Cat # 170-8841
Fast SYBR Green Master Mix	Thermo Fisher	Cat # 4385612
CD11c MicroBeads UltraPure, mouse	Miltenyi Biotec	Cat # 130-108-338
Dynabeads™ Untouched™ Mouse total T cells kit	Thermo Fisher	Cat # 11413D

REAGENT or RESOURCE	SOURCE	IDENTIFIER
Dynabead™ Untouched™ Mouse CD4T cells kit	Thermo Fisher	Cat # 11415D
Dynabeads™ Untouched™ Mouse CD8T cells kit	Thermo Fisher	Cat # 11417D
Dynabeads™ Sheep anti-rat IgG	Thermo Fisher	Cat # 11035
Dynabeads Mouse T-Activator CD3/CD28 for T cell Expansion and Activation	Thermo Fisher	Cat # 11452
NE-PER nuclear and cytoplasmic extraction reagent	Thermo Fisher	Cat # 78833
Pierce BCA Protein Assay kit	Thermo Fisher	Cat # 23227
In Situ Cell Death Detection kit, TMR red	Millipore Sigma	Cat # 12156792910
Red Blood Cell Lysing Buffer Hybri-Max	Sigma-Aldrich	Cat # R7757
eBioscienoe Foxp3 / Transcription Factor Staining Buffer Set	Thermo Fisher	Cat # 00-5523-00
Mouse IL-2 ELISA set	BD	Cat # 555148
Mouse IL-5 ELISA kit	Thermo Fisher	Cat # 88-7054-22
MouselL-13 ELISA kit	Thermo Fisher	Cat # 88-7137-22
Mouse IL-17A ELISA kit	Thermo Fisher	Cat # 88-7371-22
Mouse IFN-γ ELISA set	BD	Cat # 555138
Calcineurin Cellular Activity Assay kit, Colorimetric	EMD Millipore	Cat # 207007
Alexa Fluor 647 Protein Labeling kit	Thermo Fisher	Cat # A20173
Experimental Models: Organisms/Strains		
Mouse: C57BL/6	The Jackson Laboratory	Cat # 000664
Mouse: B6.SJL-Ptprc^{a}Pepc^{b}/BoyJ (CD45.1)	The Jackson Laboratory	Cat # 002014
Mouse: B6.129S2-Tcra^{tm1Mom}/J (TcRαβ^{KO})	The Jackson Laboratory	Cat # 002116
Mouse: B6.PL-Thy1^{a}/CyJ (Thy1.1)	The Jackson Laboratory	Cat # 000406
Mouse: B6.Cg-Tg(TcraTcrb) 425Cbn/J (OT-II)	The Jackson Laboratory	Cat # 004194
Mouse: B6NK1R^{KO}	Bozic et al., 1996	N/A
Mouse: *Tac1/4^{KO}* B6	Berger et al., 2010	N/A
Oligonucleotides		
PPT-A primers *(TAC1* mouse)	SAB-Biosciences (QIAGEN)	Unique assay ID: qMmuCID0021966
PPT-C primers *(TAC4* mouse)	SAB-Biosciences (QIAGEN)	Unique assay ID: qMmuCED0045191
Software and Algorithms		
Studio Software v2	Li-Cor	https://www.licor.com/bio/image-studio/?gclid=CjwKCAjwlPTmBRBoEiwAHqpvhQtvKpg2vp6V0lhSnJDOqnH5pHCLo9YrBaFqkZ3VXAC02UfX8qeCmRoCGolQAvD_BwE
ImageJ Software v 1.51	Li-Cor	https://www.licor.com/bio/image-studio-lite/

REAGENT or RESOURCE	SOURCE	IDENTIFIER
IDEAS v6.2. software	Andritz Group	http://www.andritz.com/resource/blob/15094/317004ed1e6f9cda9efe0a600f397037/aa-ideas-v600-user-manual-data.pdf
FlowJo v.10	FlowJo, LLC	https://www.flowjo.com/
NIS Elements v5.11.01	Nikon Instruments Inc	https://www.nikon.com/products/microscope-solutions/support/download/software/imgsfw/
AxioVision Rel 4.8	Zeiss	https://www.micro-shop.zeiss.com/en/us/system/software+axio+visionaxiovision+programaxiovision+software/10221/
GraphPad Prism v7	GraphPad	https://www.graphpad.com/